The extreme C-terminus of human Topoisomerase II alpha defines a novel bi-modular DNA tether essential for the formation of mitotic chromosomes

A DISSERTATION
SUBMITTED TO THE FACULTY OF THE GRADUATE SCHOOL
OF THE UNIVERSITY OF MINNESOTA
BY

Andrew Besançon Lane

IN PARTIAL FULFILLMENT OF THE REQUIREMENTS
FOR THE DEGREE OF
DOCTOR OF PHILOSOPHY

Advisor: Dr Duncan J Clarke

May 2012

Acknowledgements

Clarke Lab
Duncan Clarke, PhD

Hung-Ji Tsai
Katie Furniss, PhD
Andrew Grenfell
Amit Vas, PhD

Ryoko Kuriyama, PhD

Adrian Fegan, PhD

Thesis Committee
David Kirkpatrick, PhD
Hiroshi Hiasa, PhD
Sean Conner, PhD
Kylie Walters, PhD

I dedicate this dissertation to my parents.

Abstract

Topoisomerase II is the target of an important class of anti-cancer drugs, but tumor cells can become resistant by reducing the association of the enzyme with chromosomes. We have determined the mechanism of Topo IIα recruitment to chromatin and provide new insight into the formation of mitotic chromosomes. We describe the first example of what is likely to be a widespread mechanism for recruitment of chromosomal proteins involving a bi-modular element consisting of an NLS and an associated DNA tether. Catalytically dead Topo IIα is successfully targeted to chromatin, but both the catalytic activity and the bi-modular targeting element are essential for mitotic chromosome formation. Because reduced strand passage activity protects cells from Topo IIα-targeted drugs, it is likely that mutations in the bi-modular element would lead to drug-resistance.

Table of Contents

List of Tables

List of Figures

Introduction

During mitosis, the mitotic chromosome compacts ten-to-twenty thousand fold over its interphase length in order to generate a physically resolved, segregable mitotic chromosome (Belmont, 2002). In both interphase and mitosis, the lowest level of chromatin compaction requires the wrapping of DNA around histones in order to generate a 10-11nm nucleosomal DNA fiber. It is thought that the nucleosomal fiber is wound into fibers of increasing width, themselves further folded to ultimately achieve the fully condensed mitotic chromosome. The nature of these subsequent levels of chromatin organization is highly controversial. At one level, however, a feature thought to be critical to mitotic chromosome structure is visible by light microscopy: the fully condensed mammalian mitotic chromosome contains a protein axial core formed by recruitment of the enzyme Topoisomerase IIα and condensin proteins. In my PhD thesis work, I have attempted to elucidate the mechanism of recruitment of Topo IIα to the mitotic chromosome as a means of understanding this final level of mitotic chromosome compaction.

Chromosome structure: the hierarchy hypothesis

Could a mitotic chromosome arise from a disordered aggregation of DNA? The rod shape of the mammalian mitotic chromosome strongly argues against this hypothesis.

A rod-shaped chromosome must arise from a progressive, hierarchical folding of the DNA polymer. To explain this assertion, consider the arrangement of DNA in the interphase nucleus as a long DNA polymer extensively tangled upon itself. Because the DNA is not in a straight line, a given portion of a single chromosome may lie closer in space to a portion of the same chromosome that is 5 megabases away than 5 kilobases away from it. Given that the process of condensation must involve parts of a chromosome associating with other parts of the same chromosome, if each piece of DNA simply interacts with the spatially-nearest piece of DNA to achieve condensation, a disorganized blob of condensed chromatin would be the likely outcome. However, if a mechanism is proposed such that a given piece of chromatin preferentially associates first with a piece a short distance away down the polymer length, rather than with a piece that abuts it in physical space but is a much greater distance down the polymer length, this establishes an initial step in the progressive shortening of the molecule down its length, but maintains the linear organization of the chromosome at large. If a similar principle is followed through several levels of this same kind of association, it's possible to imagine an overall compaction of the order seen in the transition from interphase to mitotic chromosome.

Understanding the biochemical regulation and the physical structure of these organizational levels are the primary goals of the chromosome condensation field.

Low-level chromatin organization: DNA wrapped around histones

In a hierarchical folding scheme, the lowest levels of compaction are provided by the wrapping of DNA around histone proteins. Histones are small, positively charged proteins and bind tightly to DNA, shielding the negatively charged DNA phosphate backbone and compacting the double-stranded DNA by approximately 5-10 fold.

Histones multimerize into heterotetramers containing one molecule each of H2A, H2B, H3 and H4. The tetramer associates with a second tetramer to make the final functional octamer that coordinates 145-147bp DNA in gyres along external grooves in the nucleosome. The histone nucleosome is the only physical level of chromosome compaction that has been unambiguously defined at high resolution (Luger et al., 1997). In the 2.8Å crystal structure, the N-terminal histone tails protrude between the gyres of the DNA as wrapped around the histone, leaving them exposed to enzymes capable of post-translational modification. This provides a means for the regulation of the DNA-histone interaction and of the nucleosome structure. Thus, the nucleosome is not simply a determinant of chromosome structure, but also one of the most powerful sites of response to cellular requirements. Indeed, certain histone modifications are known to be highly specific for mitotic cells; antibodies recognizing phosphorylated serine residues on histone H3 (serines 10 and 28) have long been used as markers of mitosis by histologists.

The 30nm fiber

A packing of the nucleosomes into a thicker 30nm fiber was first proposed based on EM images of chromosomes swollen in non-physiological buffers and fixed in alcohol fixatives. These experiments showed a fiber of around 30nm (Finch and Klug, 1976; and

reviewed in Maeshima et al., 2010). Later, X-ray scattering experiments showed a regular repeating structure of the same size, appearing to corroborate the EM experiments (Langmore and Paulson, 1983).

Within the 30nm fiber literature, there are a range of models proposing various structural models for the arrangement of the individual nucleosomes within the fiber. The two dominant proposals are the one-start and the two-start/zigzag models and variations thereon. A one-start model, perhaps the most conceptually simple proposal, predicts that each individual nucleosome interacts with its adjacent nucleosome, folding the

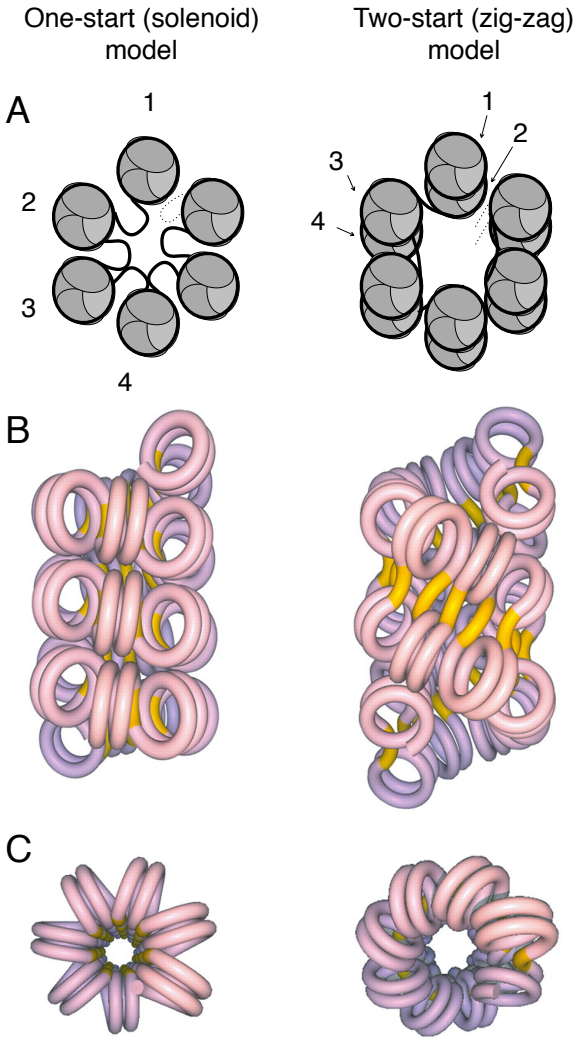

Figure 1: Two proposed models for 30nm fiber structure. Left: one start, solenoidal model. Right: Two-start, zig-zag model. A: schematic of nucleosome organization in each model, transverse view of fiber. Numbers show order of nucleosomes along DNA fiber. B: Prediction of 30nm fiber structure as viewed longitudinally. C: Prediction of 30nm fiber structure, viewed transversely. Note linker DNA (yellow) is arranged down center of fiber in one-start model, but is positioned along helix in two-start model. B and C from Dorigo, B. Nucleosome Arrays Reveal the Two-Start Organization of the Chromatin Fiber. Science 306, 1571–1573 (2004). Reprinted with permission from AAAS.

nucleosomal fiber in the process and forming a roughly 30nm fiber, later wound into a hypothetical thicker fiber (Figure 1). A two-start model proposes that each individual nucleosome interacts with the next-but-one nucleosome, with the result that a zig-zagging fiber is formed. In either model, the assembly of the 30nm fiber is thought to be dependent on and regulated by the presence of a "linker histone", usually histone H1, that "bridges" individual nucleosomes (illustrated in Grigoryev et al., 2009).

Several lines of evidence support the latter, two-start model. Most strikingly, high-resolution EM studies show zig-zagging fibers forming in the presence of linker histone (Figure 2) (Grigoryev et al., 2009; Dorigo, 2004); these can be interpreted as fragments of a two-start nucleosome fiber, which, with larger numbers of repeats, are predicted to assemble into 30nm fibers resembling that shown in Figure 2. Furthermore, a higher-order tetranucleosome structure (that is, a string of four octamers connected by linker DNA) has been shown at lower resolution (9Å) and suggests a tight stacking between nucleosomes, in which the mononucleosomes follow a zigzagged path when modeled as part of a larger stucture (Schalch et al., 2005), in agreement with the two-start model. Overall, the 30nm fiber provides for the total linear compaction of DNA by 30 to 40 fold.

The 30nm fiber may be a transient structure in chromosome condensation

The importance of the 30nm fiber in fully formed mitotic chromosomes is controversial. Cryo-EM methods allowing study of mitotic chromosomes in native state, without exposure to non-physiological buffers, suggests that the condensed mitotic chromosome is homogenous in structure; no visible repeating structure above the level of the 11nm nucleosomal fiber is seen to exist in the mitotic chromosome in these experiments (2006).

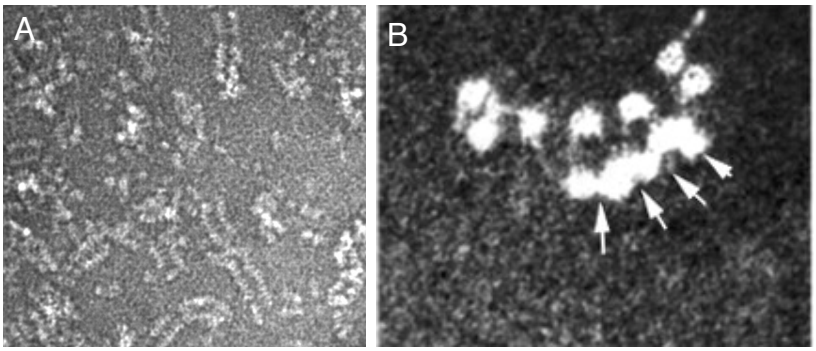

Figure 2: Electron microscopy supports the 30nm fiber two-start model. A: polynucleosomes artificially crosslinked through H4/H2A suggest that adjacent nucleosomes form a zig-zag ladder-type structure as predicted for a two-start 30nm fiber. B: In the presence of linker histone and monovalent ions, a zig-zag structure is seen. Arrows indicate associating nucleosomes.

Panel A reproduced from Dorigo, B. Nucleosome Arrays Reveal the Two-Start Organization of the Chromatin Fiber. Science 306, 1571–1573 (2004). Reprinted with permission from AAAS. (Dorigo et al., 2004). Panel B reproduced from (Grigoryev et al., 2009).

In agreement with these data, Nishino (2012) argues that previous evidence of a 30nm fiber in mitotic chromosomes by X-ray scattering is an artifact of 30nm chromatin-associated ribosome particles, as (they show) would have been contaminating samples used in previous studies. When the ribosomes are removed with modified protocols, so is the 30nm chromatin fiber "signal".

In this case, the authors hypothesize that the 30nm fiber may exist as a transient state during chromatin compaction, and is not present in the fully condensed chromosome. They model the possibility that the 30nm fiber may "melt" in the highly condensed mitotic chromosome, where nucleosomes can begin to associate randomly as overall nucleosome concentration rises above a critical value.

Cis-acting DNA elements of the organized chromosome

There is evidence that AT-rich sequences constitute *cis*-acting elements within the scaffold to which Topo II associates – the so-called scaffold attachment regions (SARs)

(Saitoh and Laemmli, 1994; Hart and Laemmli, 1998).

Central to many models of chromosome structure, particularly those involving radial loops (Figure 3), is the idea of specific DNA sequences that, at each mitosis, associate with chromosome proteins and specify subdomains of the structure. This idea has been proposed and tested in the form of Scaffold Attachment Regions and Matrix Attachment Regions. SARs were first proposed and explored by (Saitoh and Laemmli, 1994). The evidence for these regions comes from sensitive fluorescent banding experiments, which differentially stain GC-rich and AT-rich regions. The authors of this study suggest that GC-rich regions stain with a pattern showing an AT-rich "queue" that runs down the central core of the metaphase chromosome, co-localizing with Topoisomerase IIα.

A second important assumption of the work is that the sequence-selective dyes used in the study stain only AT-rich regions of the chromosome, with the same sequence basis as the well-studied Giemsa banding cytogenetics techniques. The parameters of the sequence specificity of the various dyes used have important implications for the interpretation of the AT-queue staining results. Initial evidence for this assignment (dark Giemsa bands corresponding to AT-rich regions) came from *in vitro* studies showing that, on isolated plasmid DNA in glass capillaries, certain stains bound selectively to DNA that contained above a certain threshold of AT content (Saitoh and Laemmli, 1994). Nearly a decade later, when full human genome data became available, it was possible to formally examine the relationship between Giemsa stained bands and sequence composition. Nimura (2002) found that the relationship between sequence composition and Giemsa banding was more complicated than expected. By *in silico* simulation of sequence-

selective banding, the authors showed that patterns matching the observed Giemsa staining were best recapitulated when it was assumed that dark-staining bands were a sign of *local* AT-richness, rather than absolute AT-richness. That is, a portion of a chromosome composed of 56% A/T may stain darkly in one position, but remain unstained in others. The propensity of a particular band to stain is thus determined by its AT-richness in the context of a "moving window" of total local sequence composition. Specifically, the authors found that Giemsa staining was strongly associated with any 2.5 megabase region that was especially AT- rich within the surrounding 9.3 megabases of total chromosome sequence. Whatever one might hypothesize that this says about chromosome structure, the important conclusion from these data is thus that the AT-queue, and thus the presumptive chromosome core, may not necessarily represent a strictly, consistently AT-rich set of DNA-attachments to a proteinaceous core; the criteria for staining are AT-biased, but remain fundamentally cryptic and may only be a secondary consequence of some aspect

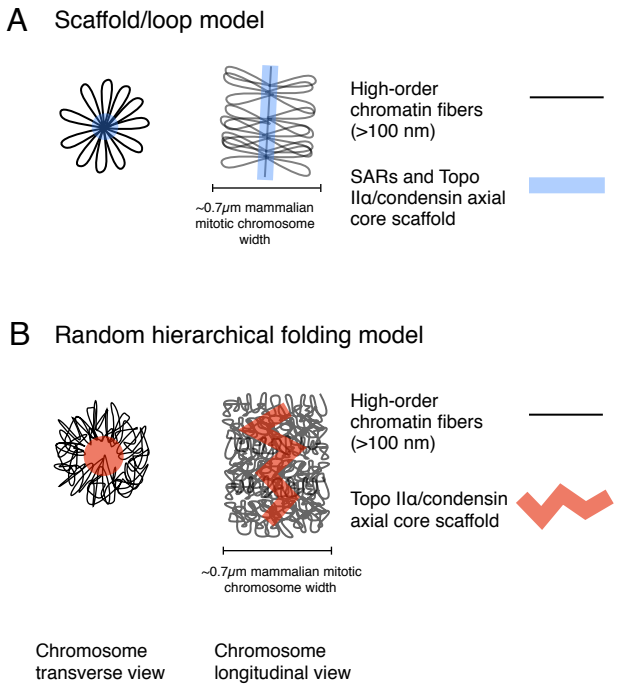

Figure 3: Higher order arrangement of chromosome structure. A: a radial loop model proposes scaffold attachment regions, specified by AT-rich DNA sequence that specifies a TopoIIα/condensin containing axial core. B: a hierarchical folding model proposes that DNA fibers are progressively folded, but do not form strict loops from the axial core. Both models account for a TopoIIα/condensin axial core. Coiling or zig-zagging of core in B reflects observations of TopoIIα/condensin localization (see Figure 7) and Maeshima (2003).

of generally AT-associated chromatin structure.

Strukov (2003) argues directly against a SAR/loop model with evidence that a large SAR-containing chromosomal insertion does not span the radial width of the chromosome, as would be expected (with the SAR at the chromosome axial core), but instead occupies a space wholly at the chromosome periphery when visualized by electron microscopy. The insertions used are larger than the predicted total size of an axial loop, and thus, under the SAR/scaffold model, would be expected to form a complete radial loop. The authors interpret this as a refutation of the simple radial loop model, and convincingly argue that these data are evidence for higher-order chromatin compaction, such that the large insertion occupies a compact volume compatible with a random hierarchical folding model (Figure 3B). A potential caveat of this work is that scaffold-association may have been incompletely specified in the authors' large chromosomal insert; in this case, and if the chromatin is compacted in unexpected ways, a place may remain for the radial loop model.

Topoisomerase IIα and chromosome structure

Topoisomerase IIα was first described as a component of the mitotic chromosome during an analysis of chicken chromosome structure (Earnshaw et al., 1985), as part of a stable protein "scaffold" structure. This protein structure persists following treatment of chromosomes with micrococcal nuclease and 2M NaCl, removing the DNA and histones, visible as a characteristically X-shaped structure reminiscent of intact mitotic chromosomes, by electron microscopy (Paulson and Laemmli, 1977; Adolph et al., 1977; Mullinger and Johnson, 1979).

Subsequent analysis showed that the scaffold is composed of two major proteins, one of which is the DNA decatenating enzyme, topoisomerase IIα (Earnshaw et al., 1985). Both topoisomerase IIα and the second major scaffold component, the CAP-E subunit of condensin, are ATPases, proposed to have roles in establishing the higher-order structure of mitotic chromosomes.

In face of the technical challenges inherent in studying the mechanism of topoisomerase IIα contribution to the structure of chromatin, much of the research into its function has been in the form of genetic analysis, particularly in yeast, or *in vitro* using purified proteins and DNA.

These studies have revealed that the enzyme is essential for cell viability. Yeast cells in which the *TOP2* gene is deleted are inviable, as are a number of *top2* temperature-sensitive alleles at the restrictive temperature (Holm et al., 1989). Similarly, it has not been possible to generate human tissue culture cell lines that are null for topoisomerase II, strongly suggesting that it is also essential in higher eukaryotes.

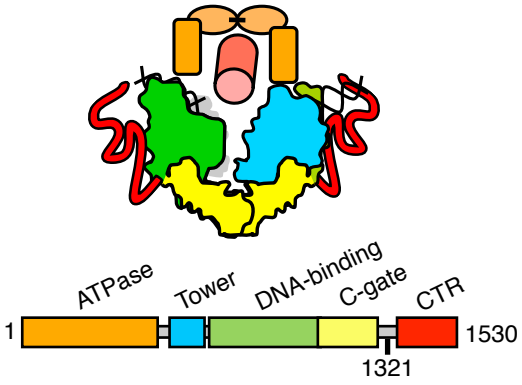

Figure 4: Domain structure of Topo IIα. Colors in upper molecular structure match those in lower domain schematic. Position of CTR in molecular structure is unknown; diagram shows one possible position. Note bent conformation of DNA (black), partially hidden by Tower/DNA-binding domains.

In the unperturbed condition, Topo II performs a strand passage reaction that makes a transient double-strand break in one DNA helix (the Gated, G-segment), passes a second helix through the break, then re-ligates the G-segment (Wang (2002), Figure 5). Topo II poisons trap the enzyme on DNA by halting the reaction cycle at

specific steps. Elegant structural studies have provided physical information on the specifics on the DNA/Topo II interaction, showing that the G-segment is positioned at the catalytic center of the enzyme by a major DNA binding core which interacts with 26 nucleotides of DNA that bend through an angle of 150˚ (Dong and Berger, 2007), suggesting that the catalytic function of Topo II relates to the enzyme's positioning within the chromosome superstructure. Strikingly, however, the DNA binding catalytic core is not sufficient for localizing Topo II to chromosomes (Linka et al., 2007). Indeed, human cells express two isoforms (Topo IIα and Topo IIβ) that have indistinguishable catalytic cycles, but only the alpha isoform is localized to mitotic chromosomes, with the beta isoform displaying only a weak localization to mitotic chromosomes in live cells (Linka et al., 2007; Christensen et al., 2002). At the level of the whole organism, the two isoforms differ in their expression pattern, with the α isoform upregulated in proliferating cells, and the β isoform appearing to be most highly expressed during development, then,

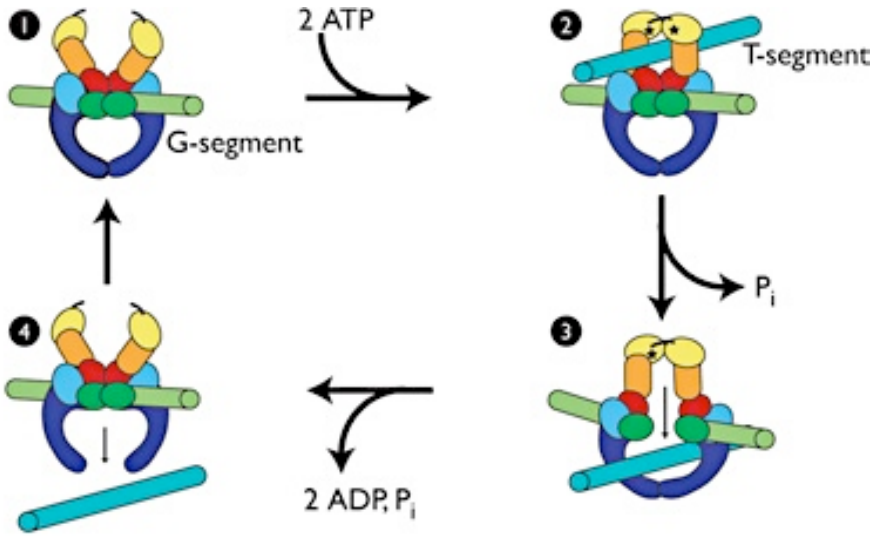

Figure 5: Topoisomerase II strand passage reaction. 1: G-segment DNA ("gate" segment, green) is captured. 2: ATP binding causes ATPase domains (yellow) to dimerize around T-segment DNA (teal). 3: ATP hydrolysis triggers DNA gate opening and passage of T-segment between ends of cleaved G-segment DNA. 4: ADP/Pi release permits liberation of T-segment DNA and returning of the enzyme to its original conformation. Figure reproduced from Schoeffler et al. (2005).

in the adult organism, as a "housekeeping" gene in non-proliferating cells (Capranico et al., 1992).

The two isoforms differ in protein sequence composition primarily in their extreme N-terminal and C-terminal regions. Linka et al. (2007) initially investigated the contribution of these sequences to subcellular protein localization using GFP-tagged proteins and found that the C-terminal 360 residues (residues 1171 to 1530) are responsible for α-isoform-specific localization.

In my thesis work, I have sought to understand the mechanistic basis of localization of Topo IIα to mitotic chromosomes in terms of specific protein sequence requirement, chromosomal binding partners and dynamics.

Understanding the mechanism of association between Topo II and chromatin is of central importance. Topo II is the target of a major class of anti-cancer drugs – Topo II "poisons" trap the enzyme on DNA; mutations that alter chromosome/Topo II interactions alter the sensitivity of cancer cells to these drugs. However, beyond the assumption that it exploits the DNA-binding portions of the protein (presumably an incomplete model because the scaffold exists following treatment with DNAse), the mechanism of Topo II targeting to the scaffold remains unknown. Key processes affected by Topo II poisons - from scaffold formation itself, to chromosome condensation and segregation - remain incompletely understood.

Although one of the first steps in the prophase assembly of the scaffold requires Topo II (Earnshaw et al., 1985; Maeshima and Laemmli, 2003), there is evidence that the axial core is formed through the re-organization of interphase nuclear matrix elements

(Berezney and Coffey, 1974; Bekers et al., 1981; Adolph, 1984) and that DNA replication may be a pre-requisite for scaffold assembly in mitosis (Berezney and Coffey, 1974; Cuvier and Hirano, 2003). However, whether molecular events coupled to replication are required for the association of Topo II with the scaffold and for chromosome condensation has only been tested in Xenopus egg extracts (Cuvier and Hirano, 2003) and it is not known if this is the case in intact cells. Upon condensation in prophase, the scaffold is initially observed as a single axial element at the center of each unresolved pair of sister chromatids (Giménez-Abián et al., 1995); the later resolution of the sisters requires Topo II and typically occurs by prometaphase (Giménez-Abián et al., 1995; Losada et al., 2002), suggesting a temporal distinction between scaffold formation and this aspect of Topo II function.

Summary of findings: The localization mechanism is a two-step process, likely initiated through its nuclear localization and stabilized by binding both DNA and histones using its extreme C-terminus.

Because alterations in localization must necessarily affect total catalytic activity, and reduced strand passage events desensitize tumor cells to Topo II poisons, a conceptual link exists between localization and drug efficacy. Determining how Topo IIα localizes to chromosome cores is also central to understanding the structural formation of mitotic chromosomes. Here we describe a novel bi-modular element in the C-terminal region (CTR) of Topo IIα that is necessary for chromosomal localization. Surprisingly, the targeting sequence contains an NLS, which may represent a general mechanism for targeting proteins to chromatin. The second component at the extreme CTR contains features necessary for a stable interaction between the enzyme and the mitotic

chromosome. We refer to this component as the Topo II DNA tether (TDT) because it facilitates stable binding of the bi-modular element to DNA in vitro. To probe the biological importance of the bi-modular element, we established a novel knockdown/ rescue system for functional analysis of Topo IIα mutants and utilized this system to determine that: (1) The bi-modular element is necessary for localization of Topo II to the scaffold and for mitotic chromosome formation; (2) Topo II catalytic activity is dispensable for scaffold association, but is required for chromosome formation.

Chapter 1

The protein sequence determinants of Topoisomerase IIα localization

To avoid DNA breakage, type II topoisomerases function as remarkably stable homodimeric enzymes (Tennyson and Lindsley, 1997). This property has hindered study of determinants that confer targeting to the nucleus in interphase and chromosome scaffold in mitosis: exogenously expressed mutants (e.g. defective in localization) bind to the endogenous protein and are targeted passively. The three dimerization interfaces of Topo II are structurally complex; this has precluded the generation of dimerization mutants. To circumvent these limitations, we characterized a heterologous system, based on an initial observation that human Topo IIα cannot be co-immunoprecipitated with the *Muntiacus muntjac* ortholog (Figure 6). To study the localization of human Topo IIα in *M. muntjac* cells, we employed a fusion protein (GFP-Topo IIα) that has been previously characterized (Tavormina et al., 2002). Fortuitously, *M. muntjac* cells have the largest known mammalian chromosomes and are thus ideal for studying structure and composition at high resolution using light microscopy. Topo IIα was primarily nuclear in

interphase cells and, in live mitotic cells, decorated the length of chromosomes with a distinctive and characteristic enrichment at centromeres (Figure 7). On chromosome arms, it localized strongly to the axial core (cf. DAPI and GFP channels in Figure 7) which was revealed as a repeating coiled punctate pattern at high magnification in fixed samples (Figure 7, lower right). This matches the localization pattern seen in other mammalian cells, when observing GFP-Topo IIα directly or using anti-Topo II antibodies against the endogenous protein (Tavormina et al., 2002; Giménez-Abián et al., 1995; Earnshaw et al., 1985).

Nuclear localization of Topo IIα depends on a non-canonical bipartite NLS

The nuclear localization signal (NLS) of Topo IIα has been reported to be in the CTR between residues 1454 and 1497 (Mirski et al., 1999 and Figure 8). We sought to validate this and to define the nature of the NLS precisely. An important caveat of previous work was the use of COS-1 (simian) cells in which simian and human Topo IIα proteins may dimerize, causing artifacts in mutant protein localization. The heterologous muntjac/ human system allowed us to circumvent this caveat (Mirski et al., 1999).

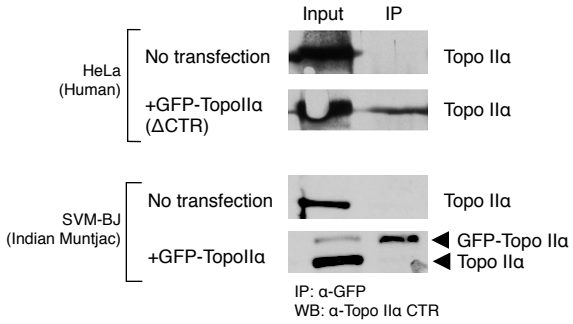

Figure 6: Human Topo IIα does not dimerize with M. muntjac Topo IIα. Top: Immunoprecipitation using GFP antibody in HeLa cell lysate from untransfected cells or cells expressing human GFP-Topo IIα E1226* (this mutant retains Topo IIα dimerization interfaces, but is not detected by the anti-Topo IIα antibody directed at the CTR and used for Western blot). Bottom: Immunoprecipitation using GFP antibody in M. muntjac cell lysate from untransfected cells or cells expressing GFP-Topo IIα.

We first made truncations from the C-terminus at 100 amino acid intervals; constructs encoding residues 1-1400 failed to localize to nuclei (as did any larger deletions of the CTR).

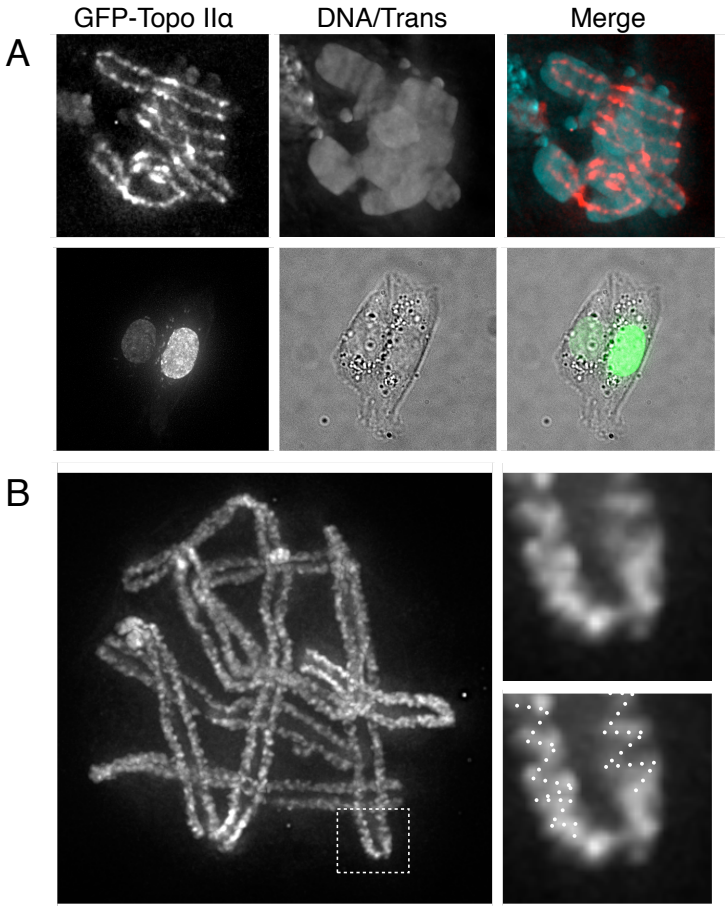

Figure 7: Topo IIα localizes to mitotic chromosome cores in mitosis and to the nucleus during interphase. A: Human Topo IIα localization in live M. muntjac cells. Top row: Metaphase chromosomes. Bottom row: Interphase nuclei. B: Left: Human Topo IIα localizes to the axial core of fixed M. muntjac chromosomes. Top right: Note punctate coiling pattern in enlarged segment of one chromosome. Bottom right: Coiling in axial core highlighted.

Constructs encoding residues 1-1500 or longer were efficiently localized to nuclei. Thus, an essential NLS lies between residues 1400 and 1500. To identify the NLS-containing sequence within this interval, we constructed C-terminal truncations at 20-residue intervals between 1400 and 1500. A construct encoding residues 1-1479 failed to localize to nuclei, thus defining an NLS that, in part, includes residues between 1479 and 1500 (Figure 8), in agreement with previous reports (Mirski et al., 1999). The bipartite NLS contains two basic regions that we refer to as NLS-A (1458-1467) and NLS-B (1479-1491) (Figure 8).

Because NLSs are known to rely on stretches of positively charged residues

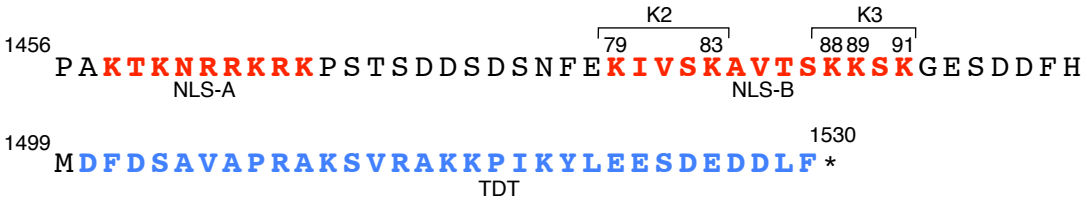

Figure 8: Primary structure of C-terminus of Topo IIα. Marked are the locations of two nuclear localization signals (NLS-A/NLS-B), two groups of lysine residues in NLS-B designated K2 and K3, and the TDT. A region describing an NLS that spans residues 1455 to 1492 has been previously described (Mirski et al., 1999); all other designations have been defined in the course of this work.

(Cokol et al. 2000; Conti et al. 1998), we mutated lysines in NLS-A and NLS-B. While the lysines/arginines in NLS-A are in a tight cluster, NLS-B can be further divided into a group of two lysines and a group of three lysines that we designate K2 and K3 (Figure 8). We mutated NLS-A, NLS-B K2 and NLS-B K3 as three separate groups to alanine. If the charge of these residues is important for NLS function, we predict that substitution to uncharged alanines would abrogate nuclear import of Topo IIα. In all three sets of point mutants, nuclear import was abrogated (Table 1). In further experiments, we found that from among the point mutations in the K2 residues, Topo IIα^{K1479A} was entirely deficient in nuclear import, whereas Topo IIα^{K1483A} translocated to the nucleus with reduced efficiency. Of the residues constituting K3, each of the individual mutants (Topo IIα^{K1488A}, Topo IIα^{K1489A} or Topo IIα^{K1491A}) showed a similar phenotype to the triple mutant, wherein nuclear import was eliminated.

Canonical NLSes rely on positively charged residues, wherein a conservative substitution between lysine and arginine may have no effect on NLS function. However, specific SUMO modification of NLS lysine residues has been suggested to alter NLS function (Chen et al. 2006). Thus, a nuclear localization phenotype seen in a lysine-to-arginine mutant may suggest a role for post-translational modification of lysines in the NLS. We constructed lysine to arginine mutants in K2 and K3 to generate Topo IIα^{K2R}

and Topo IIα^{K3R}, and found that Topo IIα^{K2R} mutants had wild-type nuclear localization (Table 1), both as a double mutant and the single K1479R and K1483R mutants. The Topo IIα^{K3R} mutant, however, showed no nuclear localization. Therefore it appears that, unlike the K2 residues, conservation of charge at the K3 residues is not sufficient for NLS function, suggesting a possible role for post-translational modification at these residues.

Chromosome scaffold localization of Topo IIα depends on elements of the NLS

We next sought to determine the residues necessary for chromosome localization in mitosis and first tested each of the mutants generated for investigation of the NLS. There was a correlation between ability to localize to interphase nuclei (i.e. NLS function) and ability to localize to condensed chromosomes in mitosis. That is, a mutant unable to localize to the nucleus during interphase (Topo IIα^{K1479A}) was also unable to localize to mitotic chromosomes (Table 1). This suggests a previously unappreciated mechanistic relationship between nuclear import and chromosome association. There is no trivial mechanistic explanation; the nuclear envelope is absent during mitosis in higher eukaryotes, obviating the need for a protein to contain an NLS to access chromosomes.

Chromosome scaffold localization of Topo IIα is not mechanistically linked to DNA replication or nuclear import

Previous studies using Xenopus egg extracts linked prior DNA replication with the association of Topo IIα with the chromosome scaffold in prophase (Cuvier and Hirano, 2003). The relationship between DNA replication and core formation has not been studied in intact cells. However, we found that although the primary sequence determinants of nuclear localization and chromosomal localization of Topo IIα overlap,

Mutant	Interphase	Metaphase
1-1530 (full-length)	Nuclear	Chromosome cores, kinetochores
1-1479	Cytoplasmic	Diffuse
1-1530 (K1479A)	Cytoplasmic	Diffuse
1-1530 (K1479R)	Nuclear	Chromosome cores, kinetochores
1-1500	Nuclear	Chromosome cores, kinetochores (labile, see text and Figure 19)
1-1530 K1488R, K1489R, K1491R ("K3R")	Cytoplasmic	Chromosome cores, kinetochores
1-1530 K1479A + SV40 NLS	Nuclear	Chromosomes cores, kinetochores

Table 1: Localization of constructs after mutating/truncating NLS and CTR of GFP-Topo IIα in *M. muntjac*, as determined by fluorescence microscopy

analysis of K3R mutants revealed that chromosome localization is not dependent on nuclear import *per se*. As described above, K3R mutants were unable to localize to nuclei during interphase. However, K3R (and K3A) mutants localized normally to chromosomes during mitosis (Figure 9). This rules out hypotheses in which presence in the nucleus during interphase is required for a "licensing" step for chromosome localization in mitosis, including models in which the deposition of Topo II onto interphase matrix components, that later form the scaffold, is mechanistically linked with DNA replication (Cuvier and Hirano, 2003). Similarly ruled out are mechanisms wherein passage through the nuclear pore is a necessary step. We considered the possibility that the K3R mutant may be successfully recruited to nuclear pores in interphase, perhaps receiving a post-translational modification necessary for chromosome localization, but is then unable to pass through the pore. However, we could see no evidence of K3R accumulation at the nuclear envelope (when compared to K1479A; data not shown). Therefore, it is reasonable to hypothesize that the K2 lysines of NLS-B, independently of their function as an NLS *per se*, are specifically able to stimulate binding of Topo IIα to components of the mitotic chromosome scaffold. Furthermore, the charged residues in K3R are sufficient for chromosomal association, whereas for nuclear

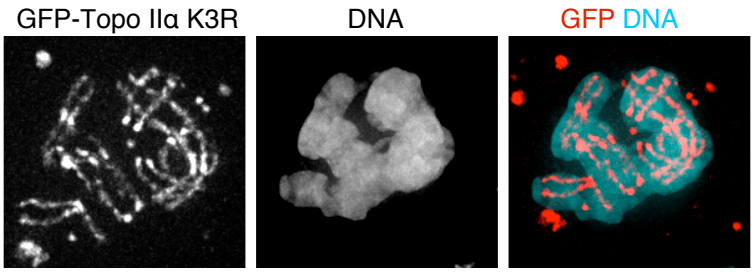

Figure 9: GFP-Topo IIα-K3R localizes similarly to WT Topo IIα in mitotic *M. muntjac* cells.

import, modifications at these positions may be important.

NLS elements function in a general mechanism of chromosomal targeting

If NLS function is truly co-opted for chromosomal localization, we reasoned that chromosomal localization of the NLS mutants (e.g. Topo IIα^{K1479A}) should be rescued by fusion of the mutant protein to the well-characterized NLS from the SV40 large T antigen. Indeed, this is what we observed: chromosomal localization was fully restored in a construct composed of Topo IIα^{K1479A} fused to a 7-residue SV40 NLS at the C-terminus of Topo IIα (Table 1).

Having defined residues necessary for chromosomal localization of Topo IIα, we next sought to determine its minimal localization sequence using portions of the CTR fused to mCherry. We tested the ability of mCherry alone to localize to mitotic chromosomes and found that, by fluorescence microscopy, it is excluded from chromosomes, visible as chromosome-shaped regions of low mCherry fluorescence that co-localize with DNA (Figure 10, top row). To further examine data suggesting a relationship between an NLS and localization to mitotic chromosomes, we generated an mCherry-SV40 NLS fusion construct. Unlike mCherry alone, mCherry-NLS was weakly enriched at chromosomes, co-localizing with DNA (Figure 10, row 2). Thus, the data indicate that, for both Topo IIα and mCherry, NLS sequences function in mitosis to

recruit the protein to chromosomes. This has not, to our knowledge, been previously experimentally demonstrated. Furthermore, these findings explain a set of related evolutionary arguments (see Discussion). We propose that NLSs can have dual function, firstly in nuclear import and secondly in chromosomal targeting.

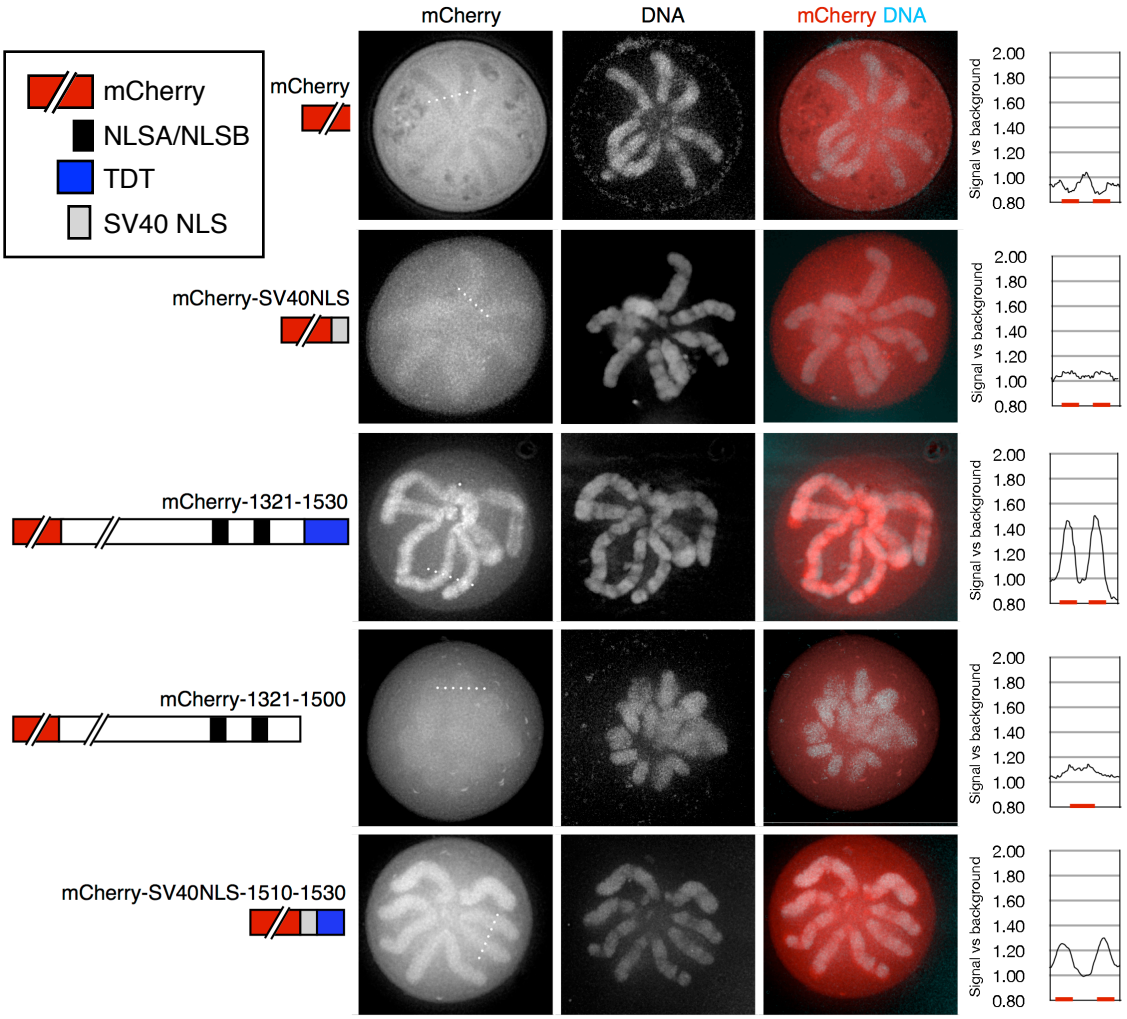

Figure 10: The extreme CTR defines a determinant sufficient for chromosomal localization
Constructs containing fragments of the human Topo IIα CTR localize to mitotic chromosomes in *M. muntjac* cells and depend on the last 30 residues. Right, line profiles over chromosomes shown in mCherry channel (dotted white lines in those images). Line profiles were calculated as mean of values from 10px on each side of line shown.

A novel bi-modular element of Topo IIα sufficient for chromosomal targeting

It was previously reported that the carboxy-terminal 25% (359 a.a. from residues 1171-1530) of Topo IIα is sufficient to direct localization to mitotic chromosomes (Linka et al., 2007). We found that this could be truncated further to a 210 a.a. fragment (1321-1530) and the localization maintained and recapitulated in the human/muntjac heterologous system (Figure 10, row 3). We truncated this shorter fragment from its own C-terminus and found that the extreme C-terminal 30 residues were essential for localization to mitotic chromosomes (Figure 10, row 4).

The data indicated that an NLS and the extreme C-terminus are necessary for localization to mitotic chromosomes. We next asked if such a bi-modular element is sufficient for chromosomal targeting by fusing the extreme CTR to mCherry-NLS. We found that a construct containing the C-terminal 20 residues of Topo IIα fused to mCherry-NLS localized efficiently to mitotic chromosomes (Figure 10, row 5). Taken together, these data indicate that chromosomal localization is directed by the combination of the NLS of Topo IIα and the C-terminal 20 residues that we refer to as the Topo IIα DNA tether (TDT).

Conclusion

There appears to be a relationship between nuclear localization and chromosome localization in the CTR of Topo IIα, and, furthermore, a general relationship between nuclear localization and chromosome localization. Furthermore, a 20-residue stretch of the extreme CTR of Topo IIα is sufficent to localize mCherry to mitotic chromosomes when fused to an SV40 NLS, suggesting that this sequence has the ability to interact with

components of the mitotic chromosome in order for it to be retained there.

The basis of the relationship between the NLS and chromosomal localization may lie in a gradient of Ran-GTP from the mitotic chromosome and co-opting of the nuclear import machinery after nuclear envelope breakdown for recruitment of proteins to mitotic chromosomes. This hypothesis is discussed further in the Discussion.

Chapter 2

The molecular mechanism of Topoisomerase IIα localization

We next sought to determine the physical mechanism of association between Topo IIα$^{1321\text{-}1530}$ and chromatin. Because Topo IIα has not been reported to physically interact with other components of the chromosome scaffold, we first investigated the ability of recombinant Topo IIα$^{1321\text{-}1530}$ fragments to bind directly to DNA: either plasmid DNA or 60bp oligonucleotides using a pair of complementary assays (Figure 12 and Figure 13).

Topo IIα$^{1321\text{-}1530}$ binds DNA in vitro dependent on the bi-modular element

To investigate binding of supercoiled and relaxed plasmid DNA, we employed the electromobility shift assay (EMSA) in agarose gels (Figure 12). Purified recombinant Topo IIα$^{1321\text{-}1530}$ or purified histone H1^{0} was incubated with pUC19 plasmid DNA containing a mixture of supercoiled, open circular and linear forms. An electromobility shift was seen in all three forms of DNA, decreasing in magnitude as the molar ratio of protein to DNA decreased. When similar fragments of Topo IIα lacking 30, 50 or 70

residues from the CTR were tested, a progressive decrease in the magnitude of the mobility shift was observed. Importantly, the DNA shifted by Topo IIα$^{1321\text{-}1530}$ remained as a tight band, whereas smearing through the lane was observed in the truncated mutants, an effect that indicates protein dissociation from the plasmid during electrophoresis (Kaer et al., 2008; Park et al., 2008; Tseng et al., 1999). Compared to histone H1^{0}, Topo IIα$^{1321\text{-}1530}$ requires approximately 6-12 times more protein to produce a shift. However, histone H1 subtypes vary widely in their affinity for plasmid (i.e. non-chromatinized) DNA, with H1^{0} having up to 19 times higher affinity than H1a (Orrego et al., 2007). Thus, the DNA affinity of Topo IIα$^{1321\text{-}1530}$ is in a similar range to histone H1 isoforms. Together with the *in vivo* experiments, the data suggest that the extreme CTR contains sequence features that confer stable binding to DNA.

Because the magnitude of an EMSA shift depends on several factors, including the net charge of a protein, its hydrodynamic volume and the affinity of the protein/DNA interaction, we sought to confirm these results using a complementary assay. We used a pulldown strategy in which we attempted to precipitate Topo II CTR fragments with oligonucleotide-coated beads. In agreement with the EMSA data, Topo IIα$^{1321\text{-}1530}$ bound to the DNA beads efficiently (Figure 13). Truncations lacking 30 or 50 residues from the CTR were pulled down with 60% and 48% of the efficiency of Topo IIα$^{1321\text{-}1530}$, respectively. Topo IIα$^{1321\text{-}1460}$ (lacking NLS-A, NLS-B and the TDT) did not detectably bind DNA.

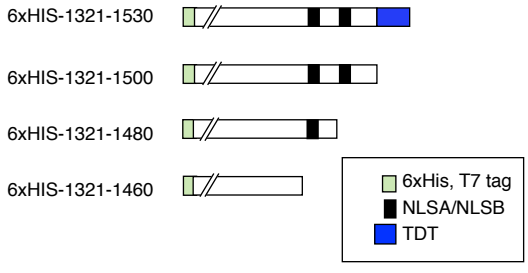

Figure 11: Topoisomerase II CTR fragments used in *in vitro* studies.

Topo IIα, but not Topo IIβ, localizes

strongly to chromosomes in mitosis. The C-terminal 25% of these proteins is the least-conserved region. To ask if the DNA binding elements in the Topo IIα CTR might be responsible for this difference, we asked if the Topo IIβ CTR binds DNA in this assay. The Topo IIβ CTR associated with the DNA beads with 10% of the efficiency of Topo IIα CTR (Figure 13). This supports the hypothesis that binding of the CTR to DNA is at least partially responsible for the strong chromosomal localization of Topo IIα.

Topoisomerase IIα binds to histone proteins *in vitro*

In addition to DNA-binding activity, we hypothesized that Topo IIα would also bind to chromosomal proteins. To investigate this possibility, we used a pulldown assay to discover binding partners of the Topo IIα CTR.

We incubated purified HIS-tagged Topo IIα CTR (complete CTR or lacking the NLSes and TDT) with HeLa cell extract and recovered bound proteins using anti-HIS

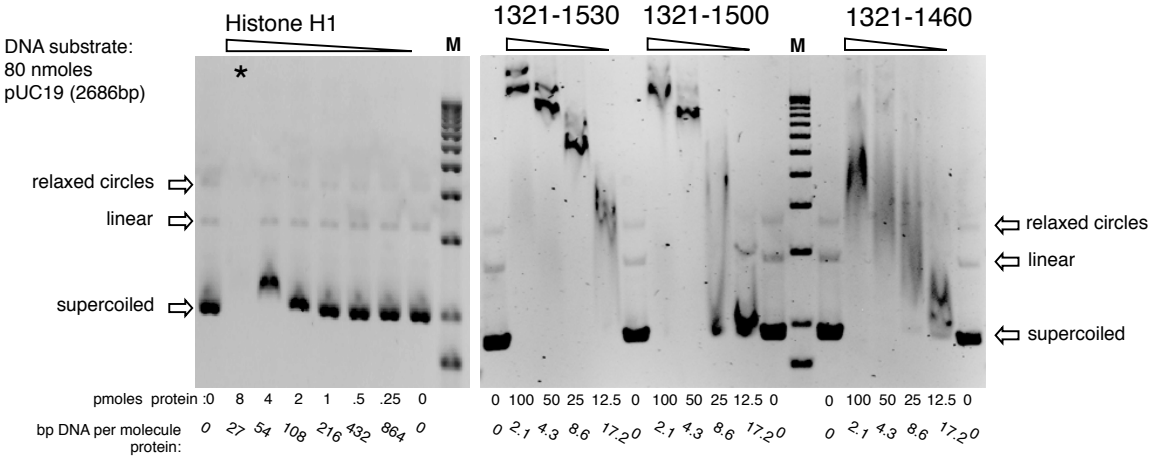

Figure 12: Topo IIα CTR binds plasmid DNA in a gelshift assay. A preparation of supercoiled, linear and relaxed pUC19 plasmid DNA was mixed with recombinant histone $H1^0$ or fragments of Topo IIα and resolved on an agarose gel. Left, Topo $IIα^{1321-1530}$; middle, Topo $IIα^{1321-1500}$; right, Topo $IIα^{1321-1460}$. M = 1kb DNA ladder.

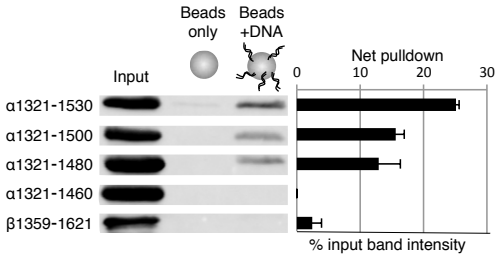

Figure 13: Topo IIα CTR binds oligonucleotide-coated beads. Blots: anti-His tag immunoblot of Topo II pulldowns using DNA-coated beads and purified HIS-tagged Topo II CTR constructs. Bars: quantification of pulldown efficiency when uncoated bead background is subtracted (% of input).

antibody-conjugated magnetic beads, then analyzed bound protein by SDS-PAGE and silver staining (Figure 14). To avoid capture of protein interactions mediated solely by DNA/RNA a promiscuous nuclease (Cynase, see Materials and Methods) was included in the extraction buffer.

Specific to the Topo IIα CTR pulldown fraction was a low-molecular weight band, suggestive of a histone protein. Subsequent Western blotting showed the presence of histone H3 in the Topo IIα CTR pulldown, but not in mock pulldowns (Figure 14B).

To investigate whether the interaction was likely to be direct, we carried out *in vitro* binding assays using full-length purified recombinant histone proteins blotted onto nitrocellulose membranes and incubuated with His-tagged Topo IIα CTR. Histones H1, H3 and H4, but not a control spot of bovine serum albumin (BSA), showed binding to Topo IIα CTR in this assay (Figure 15). We found that as little as 16nM Topo IIα CTR was sufficient to visualize binding to 1μg immobilized histone blotted onto membranes; 16nM Topo IIα CTR is equivalent to 0.432μg/ml protein. This is comparable the concentration that antibodies are used in Western blotting to detect proteins (in the range of 1μg/ml final).

We next sought to determine if this interaction was likely to be regulatable by post-translational modification of histone tails. Commercially available peptide spot

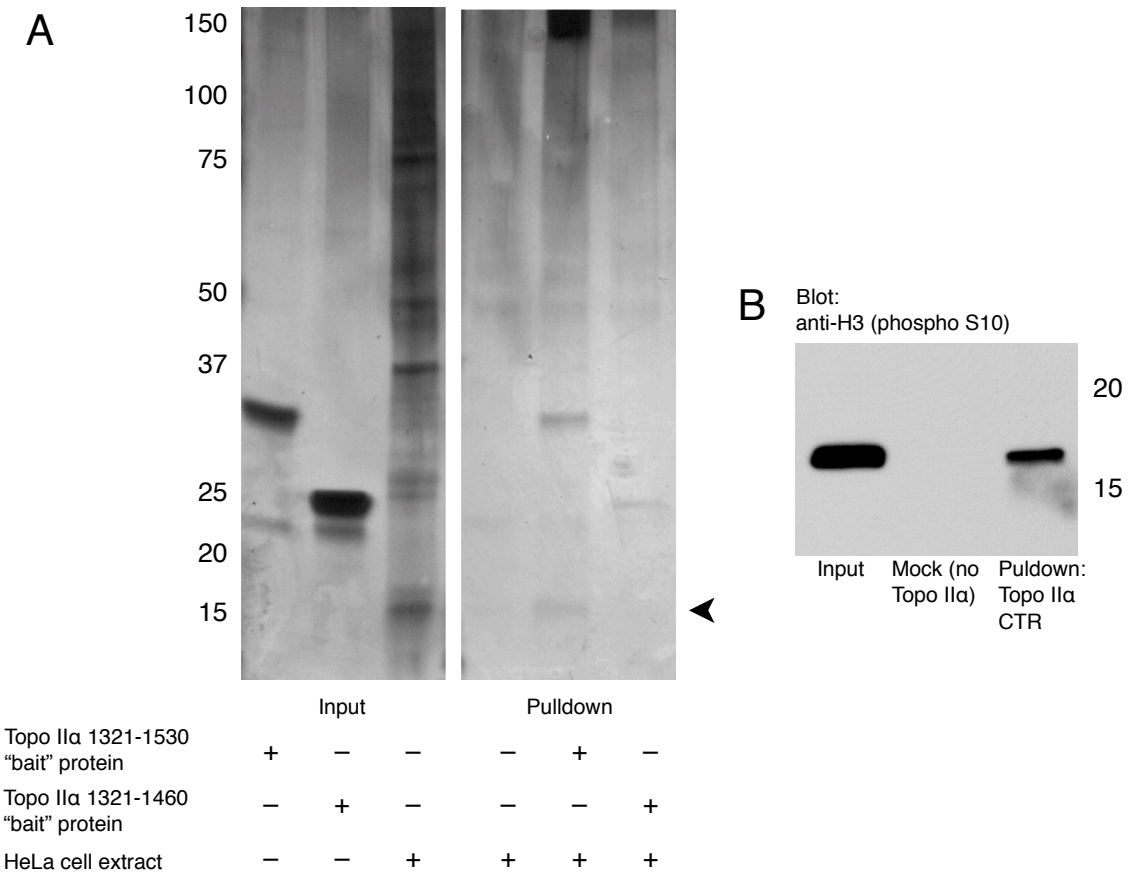

Figure 14: Histone H3 is captured in an anti-HIS pulldown from HeLa cell extract using HIS-tagged Topo IIα CTR. A) HeLa cell extract was prepared and treated with Cynase nuclease. Recombinant Topo IIα CTR (residues 1321-1530) or Topo IIα CTR lacking the NLS and TDT (residues 1321-1460) were added to extract and incubated with anti-HIS magnetic beads. Samples were analyzed on 4-20% SDS-PAGE gel and silver-stained for total protein. A low molecular-weight band was evident specifically in the Topo IIα CTR pulldown sample, marked by arrowhead. B) Mitotic cells were isolated and pulldowns performed as in A. Samples were analyzed on 15% SDS-PAGE gel and Western blotted using anti Histone H3 phospho S10 antibody. (A working pan-H3 antibody was not available).

arrays with histone tail peptides modified by methylation, acetylation, phosphorylation or citrullination at specific residues were used (see Appendix I). The array is incubated with a protein of interest (in this case, Topo IIα CTR), washed, and analyzed by standard Western blotting procedures (i.e. using antibodies against the protein of interest). Resulting spots indicate binding of the protein of interest to histone tails at that location. These spots can be cross-referenced with the known map of the array to determine the specificity of binding between modified histone tails and one's protein of interest.

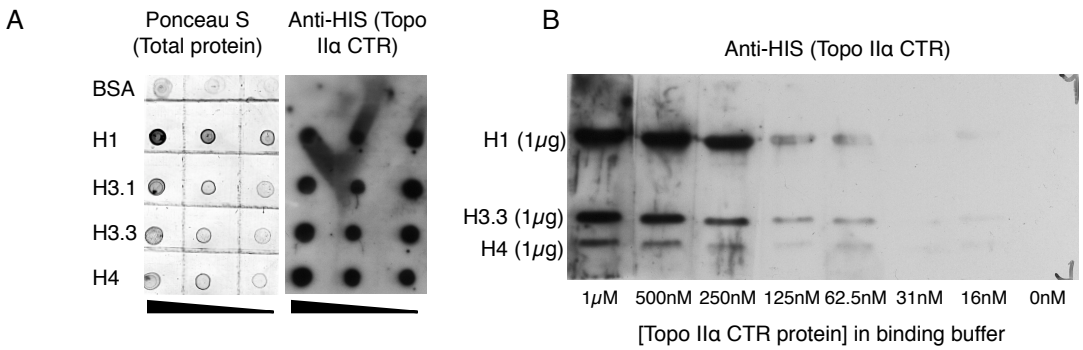

Figure 15: Topo IIα binds to histones immobilized on nitrocellulose membranes. A) BSA or decreasing quantities of histone were spotted onto nitrocellulose membrane and visualized for total protein (left), then incubated with 500nM Topo IIα CTR (1321-1530). Binding of Topo IIα to spots was detected using anti-HIS antibody. Smearing in some spots is due to excess signal in chemiluminescent assay/ movement of film. B) Similar to A, but quantity of histone remained constant (1ug), while Topo IIα concentration in binding buffer was varied over a 2-fold log dilution.

We found that Topo IIα CTR interacts with tail peptides representing H2A, H2B, H3 and H4, with some marked differences depending on post-translational modification. Each peptide array slide is arranged with two identical copies of the array (side by side) to allow an estimation of the evenness of protein binding to the slide and a calculation of the correlation between the two sides. In most cases, some unevenness of binding was apparent between the two sides (see Figure 16). However, because each histone modification is represented by more than a single spot and the overall normalized error rate is generally less than 20% between spots on different sides (Figure 16E), meaningful estimates of differences in binding can be made. In particular, Topo IIα CTR appears to bind H3 tail peptides across a broad range of modifications, with the exception that the interaction is promoted by methylation at R26 and K27, and inhibited by additional phosphorylation at serine 28 (H3S28p) (Figure 17).

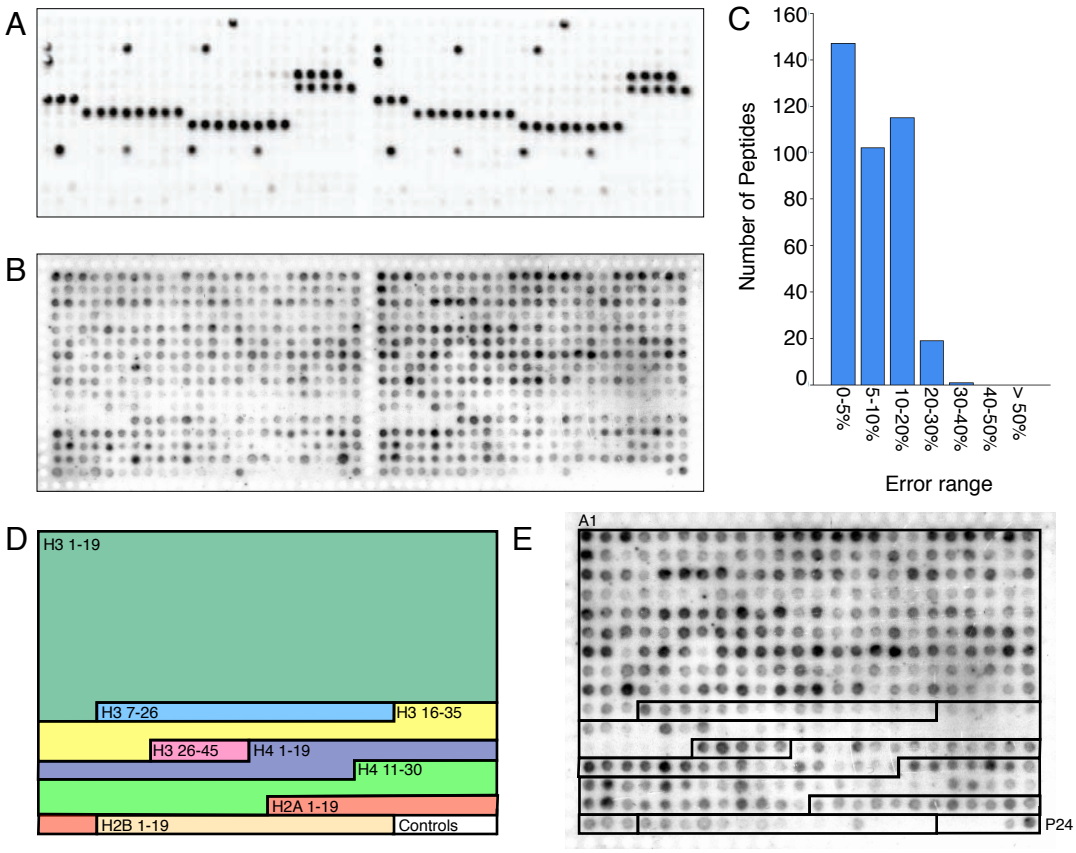

Figure 16: Histone peptide arrays can be used to probe binding of Topo IIα CTR to modified histone tail peptides. A) Manufacturer-provided example image showing reactivity of H3K9me3 antibody to spots on peptide array. Dark spots indicate antibody binding and correlate with peptides containing H3K9me3. B) Array showing binding of Topo IIα to modified histone tail peptides. Dark spots indicate binding of Topo IIα CTR to spotted modified histone tail. C) Quantification of error between two sides of array shown in panel B. Low error indicates that relative spot intensity is similar on both sides of array when normalized to control. D) Map of spotted array peptides. Within each area, histones are modified by methylation, acetylation, citrullation and/or phosphorylation (see next figure). E) Overlap of histone peptide map on right hand side of array shown in panel B.

Conclusion

Topo IIα CTR binds to both DNA and histone proteins in vitro. This binding is apparently sensitive to modification of H3 tails at specific modifications. Of particular interest is that several of the modifications are associated with mitotic chromosomes. Phospho serine 28, which these data suggest may inhibit binding, is a marker of mitotic chromosomes; it is thus surprising that this modification appears inhibitory to binding.

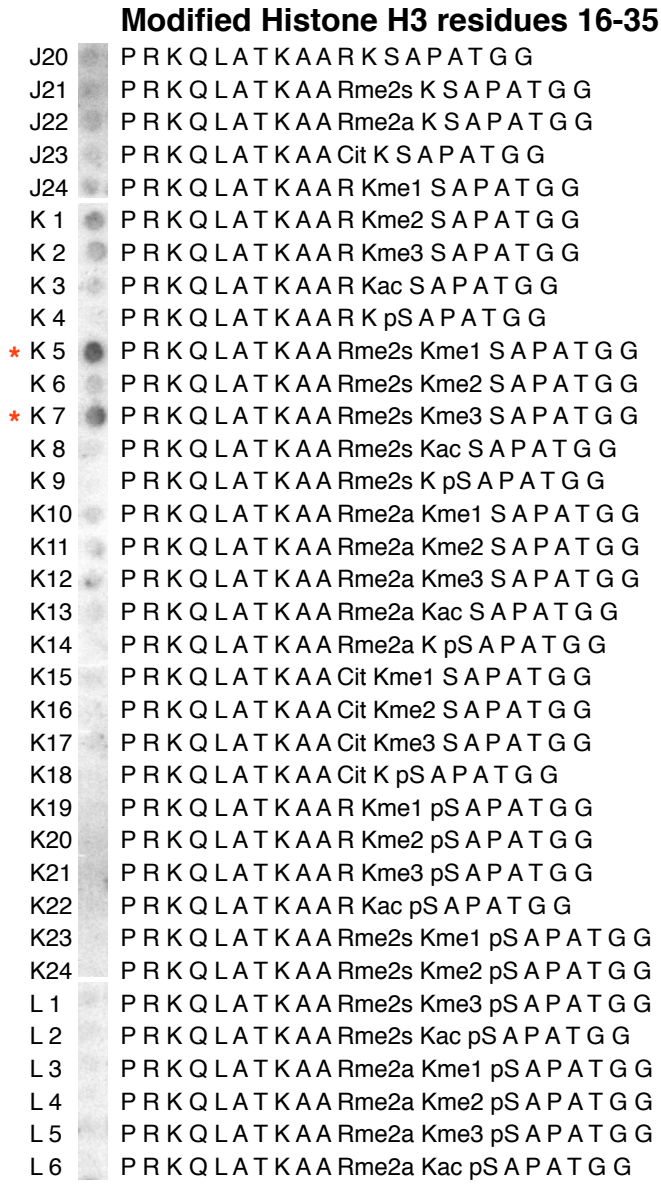

Figure 17: Histone peptide arrays can be used to determine binding preferences for Topo IIα CTR binding to a specific peptide. Spots are from previous figure spanning peptide representing H3 residues 16-35 (yellow area in panel D). In this case, K5 and K7 spots are prominent, suggesting that Topo IIα CTR associates most strongly with histone H3 tail when R26 is dimethylated and K27 is mono- or tri-methylated. When these modifications are seen in combination with phosphorylation at S28 (spots K23 and L1), the interaction appears to be abrogated. See Appendix I for analysis of remaining areas of array.

This can be reconciled by a hypothesis that implicates certain modifications in recruiting Topo IIα specifically to the mitotic chromosome (perhaps methylated R26 and K27) and using phospho H3S28 to define chromosomal subdomains excluded of Topo IIα. (for example, non-core regions). However, there are no reports of this distribution of histone modifications, as would presumably be seen using phospho-specific antibodies.

Thus far, these histone-binding data do not validate the interaction *in vivo* or

confirm any functional significance. Two important follow-up studies could be proposed: First, to study the Topo IIα/histone interaction, it would be informative to manipulate histone modification in cells and examine changes in localization or function of Topo IIα enzyme. Second, structural studies of Topo IIα CTR bound to either histone proteins, DNA or both would be informative to determine the nature of Topo IIα/chromosome component interactions.

Chapter 3

A system for the functional analysis of Topoisomerase IIα mutants

The data indicate that the CTR contains a bi-modular element necessary for Topo IIα association with mitotic chromosomes, at least in part through direct interaction with DNA and histones. Because this appears to be the first example of such an element, we sought to test biological relevance in mitosis. This was important for two further reasons. Firstly, in *Saccharomyces cerevisiae*, mutants lacking the CTR are viable (Jensen et al., 1996). Secondly, it was possible that CTR mutants undetectable on chromosomes by fluorescence microscopy nevertheless localize to mitotic chromosomes at a low level which is sufficient for function. However, the complementation of Topo IIα in cultured cells has traditionally been technically challenging. Transient transfection typically results in overexpression of the transgene leading to rapid toxicity, probably due to ectopic production of double-strand breaks. To overcome this technical challenge, we developed a system in which Topo IIα can be inducibly expressed close to endogenous levels and the endogenous protein efficiently depleted at will, allowing study of both

dominant-negative and null mutants in stable, homogenous cell lines. We combined a doxycycline-inducible transgenic Topo IIα with viral shRNA knockdown of the endogenous protein. The system employs a HeLa cell line (EM2-11ht) in which a gene of interest may be integrated stably at a well-characterized 5q31.3 "silent-but-activatable" genomic locus using the FLP recombinase (Figure 18A), thus avoiding detectable expression in the absence of doxycycline (Weidenfeld et al., 2009). Because the locus of integration was the same for all cell lines generated, the induction characteristics were similar for all mutants, permitting direct comparison of independently-derived transgenic cell lines. This enabled us to determine a concentration of doxycycline at which the level of transgenic Topo IIα was similar to that of the endogenous protein (Figure 18B).

Lentivirus-mediated shRNA resulted in depletion of endogenous Topo IIα to levels undetectable by immunoblot (Figure 18B). Transgenic Topo IIα and mutants of interest were rendered insensitive to the shRNA construct by introducing silent mutations in the target site prior to integration.

The Topo II DNA-tether is required for stability of the enzyme on mitotic chromosomes

To investigate the in vivo function of the TDT, we used the recombinase system to generate EM2-11 cell lines containing either mCherry-tagged wild-type Topo IIα or Topo IIα$^{1\text{-}1500}$ (i.e. Topo IIα$^{\Delta TDT}$). Although Topo IIα$^{\Delta TDT}$ localized to mitotic chromosomes in live cells, this association was entirely lost following fixation in formaldehyde or methanol (Figure 19). In light of data shown in Figure 10 that the C-terminal 30 residues are necessary for CTR fragment localization to mitotic chromosomes and that the C-terminal 20 residues are sufficient for strong chromosomal localization when fused to an

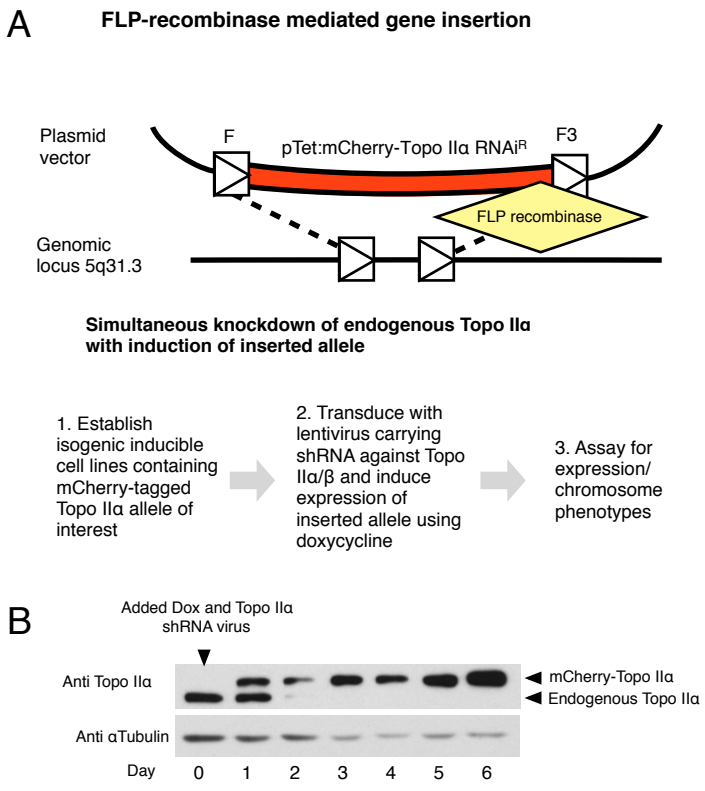

Figure 18: FLP-recombinase mediated gene insertion permits expression of mutant Topo IIα alleles at near endogenous levels. A, upper: HeLa EM2-11ht cells transfected with plasmids containing asymmetric FLP (F/F3) recombinase sites and encoding a FLP recombinase protein undergo recombinase-mediated cassette exchange (RMCE), causing simultaneous removal of the negative-selection TK gene and single-copy insertion of Topo IIα allele at locus 5q31.3 (see Methods and Weidenfeld et al., 2009). Lower: Experimental flow for generation and simultaneous knockdown/induction of endogenous and inserted Topo IIα genes, respectively. B: Topo IIα Western blot to characterize a targeted clone expressing wild-type Topo IIα from 5q31.3 under inducible control. At t=0d, doxycycline (250ng/ml) and Topo IIα shRNA knockdown lentivirus were added (5X MOI) to induce exogenous expression and deplete the endogenous protein.

NLS, these data indicate that the extreme C-terminal TDT residues are important for a full-avidity interaction with mitotic chromosomes. Since this result was the same whether or not the endogenous Topo IIα protein was depleted, the TDT must be necessary for stable scaffold association even in the presence of the endogenous protein, where the mutant is presumably able to form a heterodimer.

Localization of Topo IIα at chromosome scaffolds is independent of catalytic activity

Previous studies have shown that Topo IIα can be captured at chromosome cores with drugs that halt the enzyme's catalytic cycle, suggesting that enzyme localized there is catalytically active (Tavormina et al., 2002; Agostinho et al., 2004). However, it is not known if Topo IIα localization to chromosome cores is dependent on its catalytic activity. Others have examined this question using an overexpressed GFP-tagged Topo IIα^{Y804F}

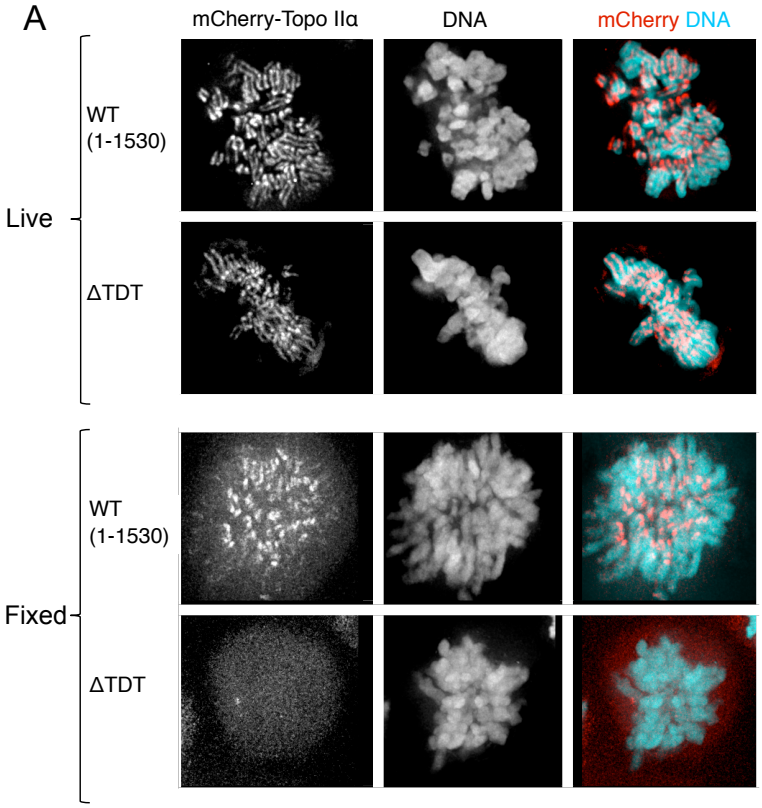

Figure 19: The Topo II DNA-tether is required for stability of the enzyme on mitotic chromosomes
HeLa EM2-11-Topo IIα cells and HeLa EM2-11-Topo IIα$^{1\text{-}1500}$ cells show wild-type mCherry-tagged Topo IIα localization in live cells, but Topo IIα$^{1\text{-}1500}$ is labile upon fixation.

mutant, where the catalytic tyrosine essential for G-segment DNA cleavage has been substituted (Jensen et al., 1996; Mo and Beck, 1999). However, those studies were carried out in the presence of the endogenous protein, thus with a population of wild-type/mutant heterodimers in human cells. The system we developed for expression of Topo IIα constructs at near-endogenous levels with knockdown of endogenous protein allowed us to address this question unequivocally. We found that the Topo IIα^{Y804F} mutant localized successfully to chromosome cores, confirming that initiation of the catalytic cycle is not necessary for localization (Figure 20). No difference in localization efficiency was seen either with or without knockdown of the endogenous protein, indicating that Topo IIα^{Y804F} homodimers localize to cores as successfully as Topo IIα/Topo IIα^{Y804F} heterodimers. These data also support the evidence that there are functional domains

outside the catalytic core important for chromosome localization. Note, however, that Topo IIα^{Y804F} retains the ability to bind G-segment DNA, and it is possible that the catalytic core of the enzyme in combination with the bi-modular element in the CTR act together to specify chromosome scaffold association (see Discussion).

Depletion of Topo II isoforms results in chromosome individualization, resolution and condensation defects

Cells treated with drugs targeting Topo IIα have been shown to have defects in chromosome condensation and segregation, indicating that Topo IIα is necessary for compaction and resolution of mitotic chromatids (Giménez-Abián and Clarke, 2009). However, drugs such as etoposide and ICRF193 exert their effects by trapping the enzyme on DNA, part way through the catalytic cycle. For this reason, the exact role of Topo IIα in these processes has not been determined. shRNA depletion allows analysis of chromosome state as a result of the absence of Topo IIα and also avoids enzyme-

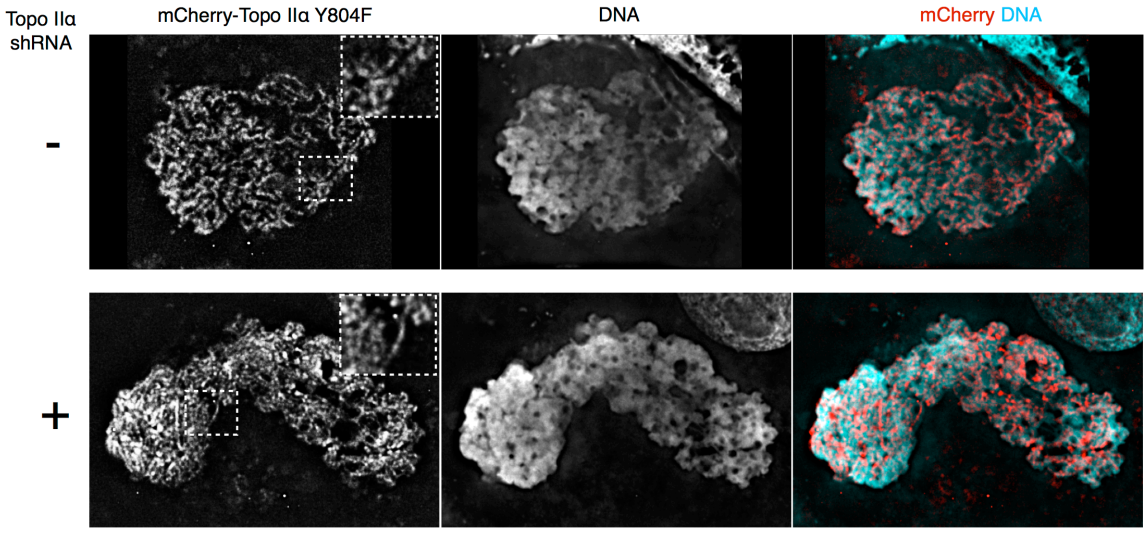

Figure 20: Localization of Topo IIα at chromosome scaffolds is independent of catalytic activity
Localization of Topo IIα^{Y804F} in late prophase/early prometaphase at chromosome cores was similar either in the presence or absence of endogenous Topo IIα. Inset shows Topo IIα along chromosome axial cores.

mediated DNA damage upon interruption of the catalytic cycle.

In pilot experiments designed to determine the experimental conditions needed to achieve lethal levels of Topo IIα knockdown, we found that cells retained some proliferative potential even on transduction with large amounts of Topo IIα knockdown virus. However, inclusion of Topo IIβ knockdown shRNA virus greatly sensitized the cells to Topo IIα depletion, while Topo IIβ knockdown virus alone had no detectable effect on cell proliferation. There thus appears to be partial functional redundancy between the two enzymes, consistent with the observed weak association of Topo IIβ with chromosomes (Linka et al., 2007). To eliminate the confounding effects of this redundancy, we conducted experiments in a background of Topo IIβ depletion.

To analyze the effects of Topo II depletion, we used HeLa EM2-11ht-Topo IIα cells in the absence of doxycycline and transduced the cells with a cocktail of Topo IIα/Topo IIβ lentiviral particles at 5X multiplicity of infection (MOI) each. Following a double-thymidine arrest protocol, we harvested mitotic cells at t=96h post transduction. While control cells treated with a non-targeted shRNA virus at the same MOI showed individualized and condensed chromosomes with well-resolved sister chromatids, cells treated with Topo IIα/Topo IIβ knockdown virus revealed a majority of cells wherein chromosomes remained as a mass of chromatin, lacking resolution between sister chromatid arms and individualization between chromosomes (Figure 21, middle and lower panels). In many of these cases, the mass of chromatin was arranged as a ring, suggesting that formation of a metaphase plate was partially successful, even though chromatids were unresolved and chromosomes not individualized (Figure 21, lower panels). A minority of knockdown cells showed chromosomes that were individualized,

but had failed to undergo complete axial compaction (Figure 21, middle right panel). This may represent a subset of cells in which only moderate Topo II knockdown was achieved.

Topo IIα$^{\Delta TDT}$ cannot promote chromosome individualization, resolution or condensation

Although Topo IIα$^{\Delta TDT}$ was not retained at chromosome scaffolds following fixation, it was present at the scaffold in live cells (Figure 19). We interpret these data to

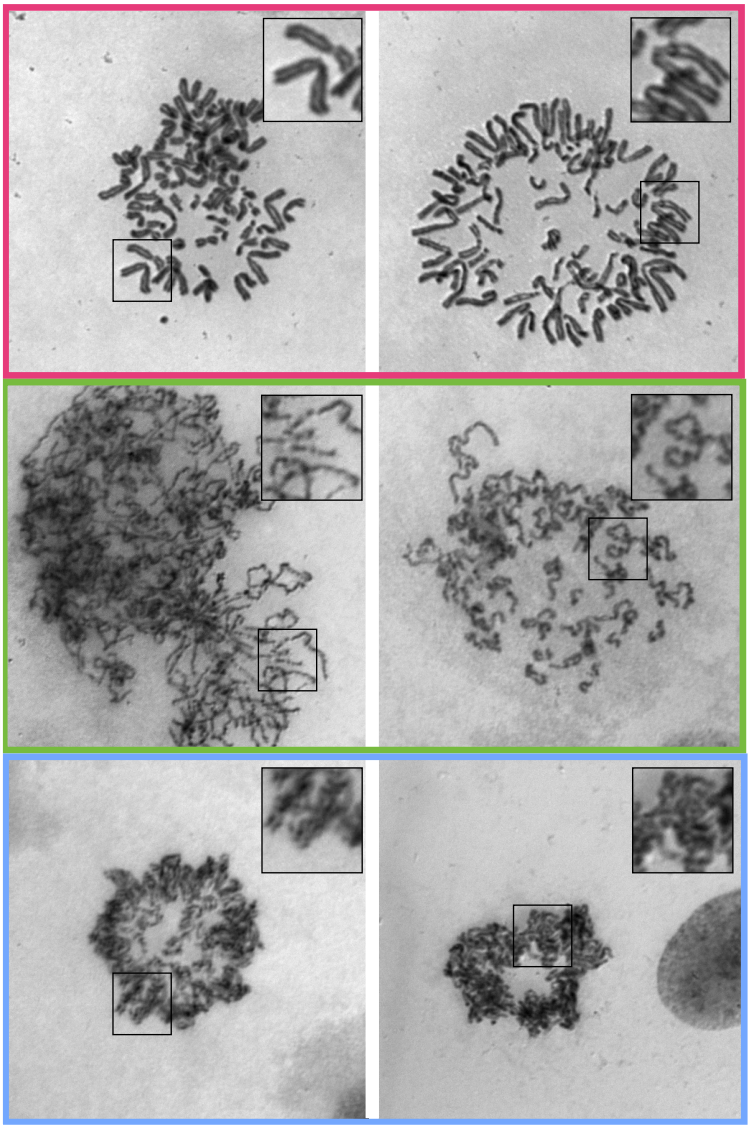

Figure 21: Depletion of Topo II isoforms results in chromosome individualization, resolution and condensation defects Chromosome spreads of Carnoy's fixed, Giemsa stained material after depletion of endogenous Topo IIα and Topo IIβ show a range of mitotic chromosome phenotypes: "Normal" metaphase plates containing individualized chromosomes were observed with visibly resolved sister chromatids (top row); Cells that failed to undergo axial compaction/condensation (middle row); failed individualization and resolution (bottom row).

indicate that Topo IIα$^{\Delta TDT}$ has reduced stability at the scaffold. It was important to ask if this reduced stability has biological significance. We therefore tested if it is possible to rescue the depletion of endogenous Topo IIα/β with activation of inserted doxycycline-inducible mCherry-Topo IIα alleles. As expected, normal chromosome morphologies were observed in most cells when wild-type mCherry-Topo IIα was induced, indicating efficient rescue of endogenous Topo IIα depletion (Figure 22). However, Topo IIα$^{\Delta TDT}$ failed to rescue the chromosome individualization, resolution and condensation defects, demonstrating that the TDT is essential for proper Topo IIα function in formation of mitotic chromosomes. Furthermore, mCherry-Topo IIα^{Y804F} similarly failed to rescue. Together the data indicate that both catalytic activity and TDT-mediated full-affinity localization are necessary for proper mitotic chromosome formation.

Conclusion

This chapter describes the establishment of a system for the functional analysis of Topo IIα mutants in live cells and shows that the TDT is necessary for Topo IIα function.

We also show that a catalytically inactive mutant of Topo IIα can localize to mitotic chromosomes, indicating that its localization there can be separated from its catalytic function. This is supported by findings in the previous chapter that the CTR alone (i.e. not including the catalytic domains) is sufficient for chromosome localization. Furthermore, the Topo IIβ isoform is not strongly chromosome localized (Linka et al., 2007), yet performs the same catalytic reaction. However, FRAP studies have shown that, while Topo IIα cycles rapidly on and off chromosomes in the unperturbed state, it does not exchange when its catalytic cycle is inhibited with drugs, and, rather, is stabilized on chromosomes (Tavormina et al., 2002). Taken together, these data support a multi-step

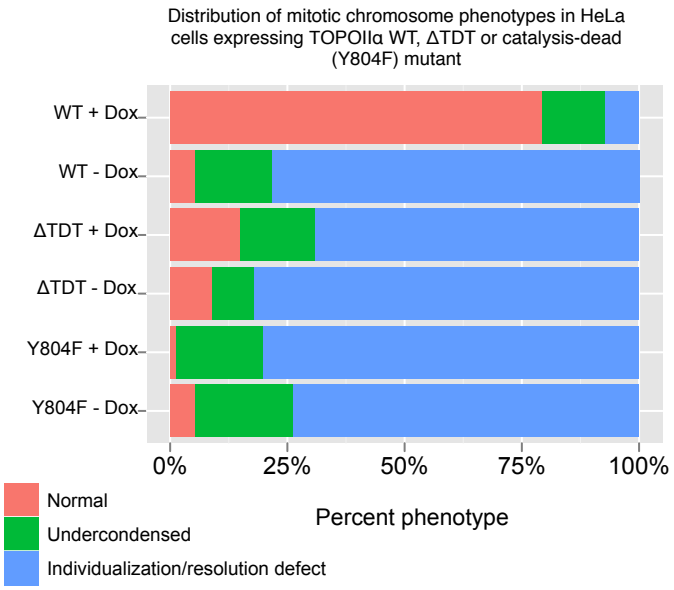

Figure 22: Topo IIα$^{\Delta TDT}$ cannot promote chromosome individualization, resolution or condensation Distribution of phenotypes seen in cells depleted of endogenous Topo IIα and induced to express WT Topo IIα, Topo IIα$^{1\text{-}1500}$ or Topo IIα$^{Y804F.}$ Categories are as described and match those shown in Figure 21.

exchange mechanism for the localization of Topo IIα, wherein initial binding at chromosomes is independent of catalytic activity, and catalytic engagement occurs as a subsequent step, at which point drug inhibition is sufficient to prevent release from chromosomes.

We have also shown that the TDT, a 30-residue sequence at the extreme C-terminus of Topo IIα, is necessary for stabilization of the protein at mitotic chromosomes. Furthermore, Topo IIα deleted of this region fails to rescue chromosome structural defects associated with loss of Topo IIα. These data indicate that a region necessary for stable association with mitotic chromosomes is also necessary for condensation of mitotic chromosomes. There are several possible mechanisms for this relationship: first, that this labile TDT mutant simply reduces the occupancy time of the enzyme at its target location (mitotic chromosomes) and simply reduces its overall activity. Second, and supported by biochemical data in Chapter 2, the TDT may be essential for interactions with other chromatin proteins (e.g. histones) that regulate chromosome structure and condensation.

The nature of these interactions, and how they coalesce to form a fully condensed, individualized mitotic chromosome, is an important question to be explored.

Chapter 4

An analysis of metaphase timing and outcome in Topoisomerase IIα knockdown cells

If the Topo IIα is necessary for resolution and condensation of mitotic chromosomes, what are the growth effects of loss of Topo IIα in dividing cells? This chapter comprises a set of analyses of the effects of Topo IIα knockdown on mitotic progression by timelapse video microscopy.

We first examined the effects of loss of Topo IIα on cell growth using the MTS assay (see Materials and Methods). This assay consists of a dye reagent which, when added to living cells in tissue culture media, is converted into a form whose maximum absorption wavelength is at 490nm. The formation of this 490nm-absorbing dye is thus dependent on the number of viable cells in a particular growth dish and can be measured using a spectrophotometer, producing a value that scales with the number of living cells in the dish.

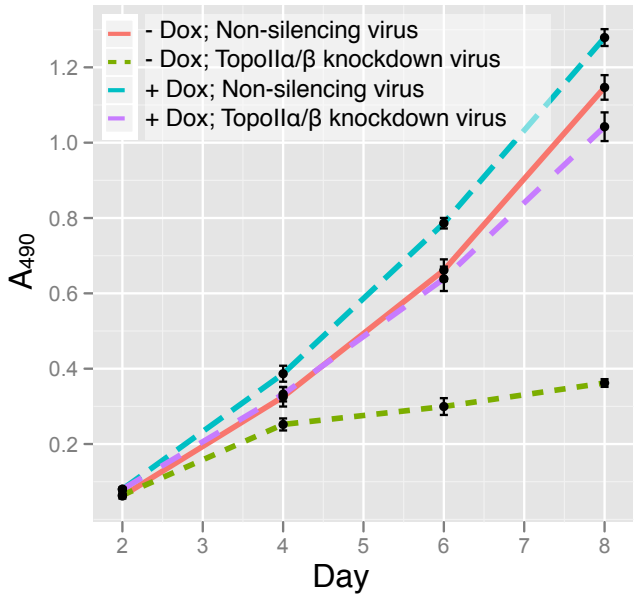

Figure 23: Knockdown of Topo IIα/β slows growth of HeLa-EM2-mCherry-Topo IIα cells (green dashed line), compared to cells transducted with non-silencing virus (red line). Induction of exogenous mCherry-tagged Topo IIα alllele using 250ng/ml doxycycline restores growth rate (purple dashed line). Teal dashed line indicates induction of mCherry-tagged Topo IIα in absence of knockdown.

We found that knockdown of Topo IIα significantly slowed the growth of cells over time and that simultaneous knockdown of both Topo IIα and Topo IIβ strongly decreased the proliferation rate of treated cells (Figure 23, green dashed line). Topo IIβ knockdown alone at equivalent virus concentrations had no apparent effect on proliferation (data not shown). Furthermore, we found that induction of the wild-type mCherry-TopoIIα allele could effectively restore the proliferation rate of cells simultaneously knocked down of both isoforms (Figure 23, purple dashed line).

Cells lacking Topo IIα likely die as a result of chromosome damage arising during mitosis

In addition to its role in mitotic chromosome formation, Topoisomerase II also has established roles in interphase, including evidence in yeast for a role resolving structures that arise in DNA replication termination (Fachinetti et al., 2010). We sought to determine if the observed slowing of proliferation was likely due to death in S-phase (suggestive that interphase roles are critical for cell survival), or in M-phase (suggestive

that mitotic roles are most critical).

To address this question, we used timelapse video microscopy of growing cells over a twenty-four hour period and compared cells transduced with non-silencing virus with those in which Topo IIα/β were knocked down. To track chromosomes, we co-transduced all cells with virus containing a histone H2B-mCherry expression construct.

We hypothesized that chromosome condensation defects would prevent chromosomes aligning correctly on the metaphase plate. The spindle assembly checkpoint remains active until this event is complete; thus, cells with improperly condensed or improperly resolved chromosomes are expected to remain in prometaphase/ metaphase for an extended period compared to control cells. We measured and quantified this period, and found that control cells spend a mean of 44.1 minutes in prometaphase/ metaphase, while Topo II knockdown cells spend a mean of 128.3 minutes; $p = 4.4 \times 10^{-6}$

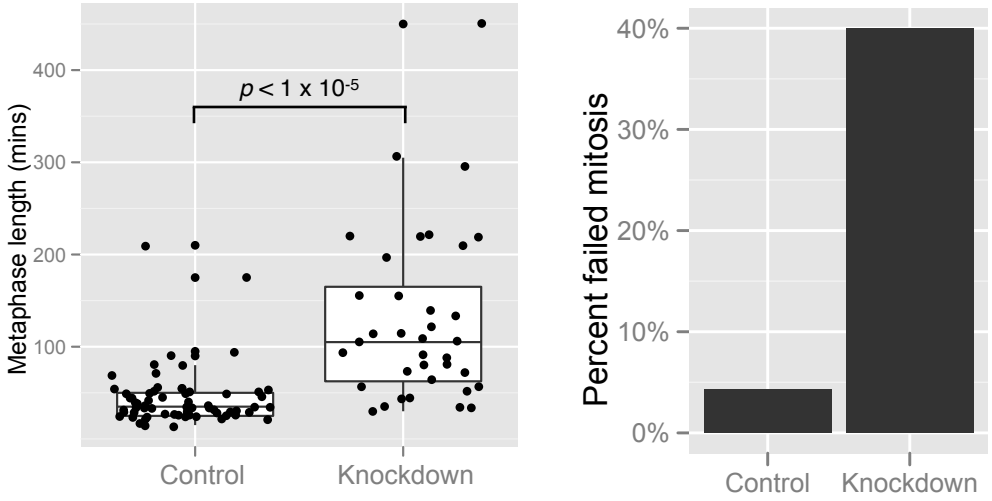

Figure 24: HeLa cells depleted of Topo IIα/β spend longer in mitosis than control cells and exhibit more mitotic defects. Control cells were treated with non-silencing virus; knockdown cells were treated with an equivalent amount of Topo IIα/β knockdown virus particles. All cells also expressed H2B-mCherry to track cell cycle progression and were monitored by timelapse fluorescence microscopy to score time spent in metaphase and outcome of mitosis. In right panel, "failed mitosis" includes cells that die during metaphase, die immediately following anaphase, or re-enter G1 from metaphase without going through anaphase.

by two-sample t-test (Figure 24). A proportion of these cells either die or re-enter the cell cycle without division; this proportion measured 4.3% in the control cells and 40.0% in the Topo II knockdown cells.

It has been well established that cells treated with topoisomerase II drug inhibitors exhibit a G2/M delay, distinct from DNA damage or other G2 checkpoints (Downes et al., 1994). We considered the possibility that this checkpoint would also be activated when cells are depleted of the Topo IIα/β enzymes. The Clarke lab's recent unpublished work in yeast indicates that this checkpoint relies on signaling through Topoisomerase II itself, rather than some secondary effect of lack of Topo II activity. Furthermore, work in mammalian cells describes an essential serine phosphorylation in human Topo IIα that is necessary for activation of this checkpoint (Luo et al., 2009). These data lead to a hypothesis that simply knocking down Topo IIα is not sufficient to activate the checkpoint. We tested this hypothesis by synchronizing control and Topo IIα/β knockdown cells at the beginning of S-phase using a double thymidine block (see Materials and Methods), and measuring the time of mitosis onset under each condition. The resulting population showed two peaks of cells entering M-phase; we interpreted the earlier, lower peak to be due to an imperfect synchrony. There was no significant difference between the two populations, suggesting the Topo II checkpoint is not activated in the absence of the enzyme (Figure 25).

Conclusion

These data suggest that the primary role of Topo IIα is at mitosis. In Topo IIα-depleted cells, events from G1 to M-phase entry appear not to be delayed, but mitosis is clearly

prolonged and correlates with death of a large percentage of cells. Furthermore, these data suggest that no other checkpoints are activated between S-phase and mitosis onset in these cells, for example, the replication or DNA-damage checkpoints. However, these data do not represent a substantial analysis of S-phase progression. Reports that Topo II has important roles in S-phase in yeast, resolving structures that arise at replication termination (Fachinetti et al., 2010), may indicate that chromosomes in Topo II-depleted cells enter mitosis with damaged chromosomes that later manifest as death at mitosis; apparent mitotic defects may arise from events occurring much earlier. This specific hypothesis will be testable using the Topo IIα-K3R mutant. This mutant is excluded from interphase nuclei, but localizes to mitotic chromosomes, providing a potentially useful tool for examining the relative importance of interphase and mitotic Topo IIα functions.

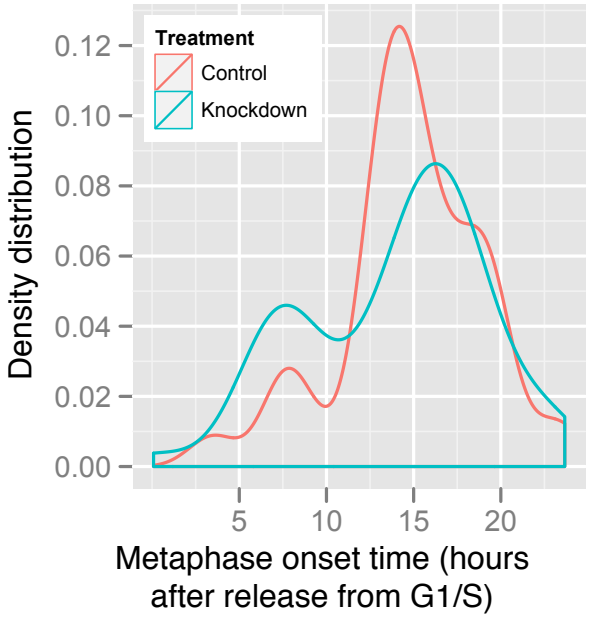

Figure 25: Control and Topo IIα/β-depleted cells enter mitosis after similar lengths of time following release from G1/S synchrony. Red line: cells transduced with non-silencing virus. Green line: cells transduced with equivalent amount of Topo IIα/β knockdown virus particles. All cells also expressed H2B-mCherry to track cell cycle progression and were monitored by timelapse fluorescence microscopy to score time spent in metaphase.

Discussion

A major research effort endeavors to maximize the efficacy of Topo II-targeted cancer drugs, but tumor cells with reduced strand passage activity become drug-resistant (Nitiss, 2009). This can occur through reduced DNA binding, making it important to understand the mechanism of Topo IIα recruitment and stability at the axial core. Studies of protein dynamics on chromosomes reveal that, paradoxically, the protein exchanges rapidly in live cells (Tavormina et al., 2002). Whether these results are explained by the existence of two pools of the enzyme – one stable and one dynamic – or by a single pool that is stabilized during the biochemical purification of scaffolds, requires more insight into the mechanism of recruitment to chromosomes. We have discovered a novel bi-modular chromosomal localization determinant in Topo IIα that employs a C-terminal 30-residue DNA tether in combination with an NLS. The bi-modular element is sufficient for efficient chromosomal targeting, is necessary for axial core localization, binds directly to DNA and histone in vitro, and is essential for mitotic chromosome formation.

To our knowledge, this is the first example of a chromosomal localization signal

of this type. The chromokinesin hKid has been shown to associate with chromosomes more dynamically in the absence of its NLS and targeting to chromosomes in part depends on the Ran-dependent machinery of nuclear localization (Tahara et al., 2008). Those studies also provided evidence that Ran-GTP induces dissociation of hKid from importins in the vicinity of chromosomes (Tahara et al., 2008). However, our data reveal an absolute requirement for the Topo IIα bi-partite NLS for chromosome targeting and demonstrate the sufficiency of a combination of an NLS and a short 20-residue DNA-tether in direct targeting to mitotic chromosomes. That it has only two short primary amino acid sequence requirements suggests that it may be a widely applicable mechanism for chromosomal localization.

When the TDT is fused to an SV40 NLS, we find strong enrichment on mitotic chromosomes. The TDT is required for a full-affinity interaction with both DNA in *in vitro* binding assays and with mitotic chromosomes in the context of full length Topo IIα. Because a crystal structure including the CTR of human Topo IIα does not exist, we are limited to speculating on its likely tertiary structure. The primary amino acid sequence of the TDT contains a stretch of acidic residues which are not predicted to bind to DNA – the C-terminal 10 residues are mostly acidic (LEESDEDDLF). It may be that surrounding a motif necessary for DNA binding with non-DNA-binding residues is necessary for coordination of binding to histone proteins.

The Topo IIα NLS is unusually sensitive to mutation at a single amino acid, the K1479 position. Although maintaining charge by mutating this to an arginine residue apparently has no effect on its function, mutation to an alanine residue (neutral) completely abrogates nuclear localization. In contrast, the K3 residues (K1488, K1489,

K1491) are absolutely sensitive to mutation to arginine residues. This suggests that these residues become modified, in which case post-translational modifications would be necessary for nuclear localization. Consistent with this notion, non-proliferating cells are able to accumulate Topo IIα in the cytoplasm (Mirski et al., 2007; Engel et al., 2004).

Although this study is the first to experimentally demonstrate the involvement of an NLS in biologically relevant and direct DNA binding, there are compelling theoretical reasons why NLSs may reside near, or within, DNA-binding regions. At the evolution of the nucleus, it was advantageous to target DNA-binding proteins for nuclear import, resulting in DNA-binding regions gaining secondary function as NLS sequences (LaCasse and Lefebvre, 1995; Cokol et al., 2000). Later, the close linkage of the two functions would retain evolutionarily benefit – new orthologs that inherited both functions would be more likely remain functional than new proteins with just one or the other, even if the sequence elements became functionally separable (LaCasse and Lefebvre, 1995). Large-scale analysis of the proximity of NLSs and DNA binding regions indicates that DNA-binding regions frequently contain NLSs (LaCasse and Lefebvre, 1995). Still, these data do not distinguish between the evolutionary advantages of linkage and a persistent functional link between DNA binding and nuclear localization. Our characterization of the relationship between an NLS and its DNA binding/chromosomal localization activity represents the first experimental demonstration of a functional link.

We note that it is not possible to fully recapitulate the localization pattern of full-length Topo IIα by expressing only CTR fragments - the bi-modular element does not specify restriction to the chromosome scaffold. It is possible that the catalytic core provides the specificity necessary for restricting Topo IIα to the scaffold. Alternatively,

the bi-modular element in isolation may have a more promiscuous affinity for DNA and thus distributes throughout the chromosome. Either way, we have demonstrated that the bi-modular element is necessary for scaffold localization. Given that the NLS is required for chromosome localization, we propose a multi-step model for loading in which the bi-partite NLS initially facilitates the permeation of Topo IIα into chromosomes, presumably dependent on the chromosomal Ran-GTP gradient (Hetzer et al., 2002; Kalab et al., 2006), as is the case for hKid (Figure 26). Once released by importin at high Ran-GTP, and thus concentrated within the chromatin, the bi-modular element then mediates DNA/histone binding and localization specified to the chromosome axis by the catalytic core, though not requiring catalytic activity (Figure 20). The bi-modular element therefore either mediates the initial interaction with DNA/histone or is essential for stabilizing Topo IIα at scaffold regions once the catalytic core has established an interaction with DNA/histone. It is possible that the bi-modular element has a role in inducing or maintaining the DNA conformation that aids the interaction at the catalytic core; a 150˚ bend is introduced into the G-segment DNA on association with Topo IIα (Dong and Berger, 2007).

Presumably, the catalytic core of Topo IIα has high affinity for DNA. This makes it somewhat surprising that further protein features are required for chromosomal localization. As mentioned above, the localization of Topo IIα to mitotic chromosomes is paradoxical, with well-accepted evidence both for Topo IIα in a structural role as part of a highly stable chromosome scaffold and, in live cells, the rapid recovery of GFP-tagged protein in FRAP experiments. Taken together, it suggests a dynamic scaffold whose aggregate structure is highly stable, but with a continual exchange of individual subunits

within it. In this model, harvesting mitotic scaffolds halts the exchange of subunits. This may happen upon plasma membrane disruption either through the loss of an ATP source needed for release of scaffold subunits or through the disruption of an intracellular gradient necessary for recruitment or replacement subunits to the chromosome; intriguingly, others have reported an increase in Topo IIα axial core localization following hypotonic treatment of live cells (Christensen et al., 2002), in which case intracellular gradients would presumably be disrupted. Taken with the relationship between the NLS and chromosomal localization, this hypothesis predicts involvement of the Ran-GTP gradient in recruitment of the protein to chromosomes, and thus would

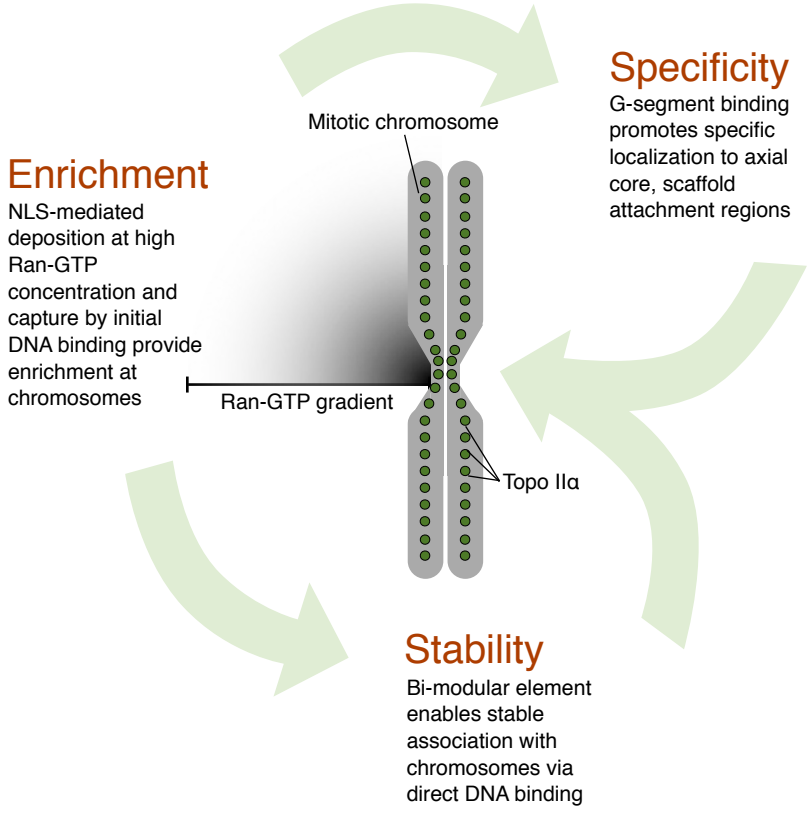

Figure 26: Model for the mechanism of Topo IIα association with chromosome cores
Enrichment at chromatin is facilitated by Topo IIα NLS sequences: first via release from importin at high Ran-GTP conc., then via DNA interaction. Specificity for AT rich DNA within the scaffold is conferred by the catalytic core of Topo IIα, which binds G-segment DNA (Figure 1, Figure 5). Stable interaction with DNA, required for formation of mitotic chromosomes, is provided by the bi-modular element (NLS + TDT) (Figure 10, Figure 19).

position this gradient as central to the proper assembly of the chromosome scaffold.

In describing the mechanism of Topo IIα recruitment to the mitotic chromosome scaffold, this work provides new insight into the formation of mitotic chromosomes. Catalytically inactive Topo IIα can associate with the chromosome scaffold but cannot promote mitotic chromosome formation. Therefore, Topo IIα does not merely serve as a structural component during chromosome condensation, individualization and resolution. Importantly, we have also described the first example of what is likely to be a widespread mechanism for recruitment of chromosomal proteins involving a bi-modular element consisting of an NLS and an associated DNA/histone tether. Because reduced DNA cleavage activity protects cells from Topo IIα-targeted drugs, it is likely that mutations in the bi-modular element would lead to drug-resistance. Such mutations would be important to identify.

Materials and Methods

Transfecting Indian Muntjac Cells with Topo IIα

Using polyethylenimine instead of GenJet or Lipofectamine means that this transfection method can be carried out on a large scale much more cost-effectively. And, moreover, other protocols don't seem to improve the transfection efficiency appreciably. There are additional benefits to using PEI, in that it probably also introduces smaller amounts of DNA into each cell, helping to reduce overexpression toxicity. When this protocol works as it should, there should be little to no visible cell death 48h post-transfection. Also, when this protocol is tested with a GFP or mCherry control vector, almost all cells are transfected; the low efficiency thus seems to be specific to Topo IIα transfection.

Grow and transfect the SVM-BJ cells in 20% serum, with 1X non-essential amino acids supplement if available (this may not make a difference). They double much more rapidly in 20% serum than in 10%.

Protocol

Day 0 For each construct to be transfected, split $3x10^6$ cells into a 10cm dish. Making sure the cells are the right density is critical; too few cells and the transfection will be toxic. This amount of cells gives an extremely dense dish, but seems to be optimal.

Day 2 For each construct, prepare in sterile 1.5ml tubes as follows (Tube B can be prepared in a larger batch). Note that PEI in the -80˚C freezer is at 10X and must be diluted to 1X with water before use.

Tube A	10cm plate
Plasmid DNA	7.35μg
150mM NaCl	to 600ul

Tube B	10cm plate
1mg/ml PEI in H_2O	22μl
150mM NaCl	600ul

Add tube B to tube A; vortex well. Incubate in hood for 20 minutes. Mix tube by pipetting up and down a few times, then add the mixture to plate of cells, drop by drop over plate surface. Place cells back in incubator overnight.

Day 3 Cells will be fully confluent by now. Split each 10cm dish into two 15cm dishes (or some into glass-bottomed dish for interphase analysis, if desired).

Day 5 Assay for expression.

Notes:

- Expression may be seen on day 4; if short for time, expression can be assayed then instead.

Small-scale extraction of Topo IIα from mammalian cells

Topo IIα is tightly associated with mitotic chromosomes in living cells; in order to completely solubilize it, extraction with SDS is necessary. Simply boiling a cell pellet in 1X Laemmli loading buffer achieves this satisfactorily, but leaves the genomic DNA in tact resulting in a viscous sample that is difficult to load and which streaks through the SDS gel if loaded. At larger sample volumes (>~150μl), the DNA can be sheared by sonication. However, this is difficult for large numbers of samples or when the sample is in a small volume. For these reasons, this protocol that uses enzymatic digestion of the DNA is a convenient alternative and ensures that all Topo IIα is extracted.

Reagents required

1. HeLa or Indian Muntjac cells; one moderately dense 6cm plate is enough for approx 5 minigel lanes using this protocol.
2. Ice bucket
3. Rubber scraper to detach cells
4. CCLB (Cynase-compatible lysis buffer)
5. Cynase endonuclease (RiboSolutions, Inc, Cedar Creek, Texas)
6. 6X Laemmli loading buffer
7. SDS polyacrylamide gels

Recipe:

CCLB (Cynase-compatible lysis buffer)		
Final composition	**For 500ul**	**Explanation**
1% Triton X-100	50μl 10%	Lyses cells
25mM NaCl	2.5μl 5M	Prevents protein aggregation (more is inhibitory to Cynase)
50mM Tris pH 8.0	25μl 1M	Buffers sample
10mM $MnCl_2$	5μl 1M	Necessary for Cynase activity ($MnSO_4$ can be used in place of $MnCl_2$, but it interferes with BCA assay)
50U/ml Cynase	50μl 0.5U/ml (i.e. 1:100 dilution of 50U/ml stock)	Degrades cellular DNA/RNA
	365μl H_2O	
(optional) Proteinase inhibitors (e.g. Complete)	*To 1X*	*Prevents protein degradation*

Protocol (6cm dish)

1. Aspirate media from cells. Wash with 1ml DPBS.
2. Add 500μl DPBS; dissociate cells from dish using rubber scraper
3. Add additional 500μl DPBS; swirl around to ensure all cells are dissociated. Transfer into 1.5ml tube
4. Spin 1.5ml tube in mini-centrifuge, 15s. Remove supernatant.
5. (Cells can be washed again here to remove all serum proteins if desired; this is not usually necessary).

6. Add 30μl CCLB to cell pellet and quickly resuspend by pipetting. Incubate on ice, 5-15 mins to lyse cells. If accurate protein concentration is required, BCA assay can be used here for quantitation; in that case, aim to load 2-10ug total protein per lane.
7. Add 50μl ddH_2O, 20μl 6X loading buffer (used as if 5X to account for cell pellet volume).
8. Boil samples, 5min.
9. Spin 3min, max speed, to remove insoluble particles.
10. Load 20μl on 6% SDS-PAGE gel; run at 200V.

Transfer of Topo IIα for Western Blotting

Transfer of Topo IIα to PVDF membrane has often been inefficient and required overnight low-voltage transfer conditions in our lab, followed by subsequent extended antibody incubations to detect the protein. Poor transfer efficiency is probably for two reasons: both its relatively high molecular weight and its high net positive charge at transfer buffer pH as a DNA-binding protein.

Because transfers are generally done under conditions where SDS is stripped from proteins, and the proteins are thus at their native charge, proteins that are not natively negatively charged at the pH of the standard Towbin transfer buffer (approx. pH 8.3) will fail to migrate during transfer. Human Topo IIα is approximately neutral at this pH, and presumably only migrates due to residual bound SDS from gel electrophoresis (or by passive diffusion…). The problem is compounded by the large size of the protein: the standard 20% methanol content of Towbin transfer buffer facilitates binding of proteins to PVDF and nitrocellulose membranes, at the expense of impeding migration of proteins out of the polyacrylamide gel. Methanol causes the gel to dehydrate, shrinking its pores.

This protocol therefore makes use of a transfer buffer with a higher pH and a lower methanol content than the standard buffer; it is based on one originally designed for transfer of histones (Szewczyk and Kozloff, 1985), albeit with 20% methanol and a higher buffer concentration in that version. The version below allows rapid and efficient transfer in one hour instead of overnight as is necessary for efficient transfer in Towbin buffer. It also has the advantage of omitting the usual glycine, and thus being less

expensive to prepare. Because the transfer efficiency is better, a one-hour incubation with antibody (Santa Cruz H-231) is sufficient to detect the protein.

Recipe

2.37g	CAPSO
1.2ml	5M NaOH
50ml	Methanol
q.s.1L	H_2O

Final: 10mM CAPSO pH 10, 5% methanol

pH should be checked the first time this is made and quantity of NaOH adjusted if not correct. Can be made as a 10X stock and stored at 4˚C. The amount of methanol can be adjusted, too. For example, for histones, 20% methanol seems to work well.

Protocol

1. Assemble Bio-Rad Mini Protein II transfer tank as standard, including ice block and a stir bar.
2. Wet PVDF membrane in methanol and equilibrate both polyacrylamide gel and membrane in transfer buffer for 5-10 minutes on shaker.
3. Assemble transfer stack in a tray under buffer as standard, taking care to remove any bubbles.
4. Place transfer apparatus in cold room on a stir plate. Transfer at 125V for 1 hour. The amperage on the power supply should read approx 350-400 mA and the buffer should

only be slightly warm at the end of the run. Increasing to 150V rapidly heats the buffer, and is thus not recommended.

Stripping PVDF Western blots for re-probing

This protocol is from (Yeung and Stanley, 2009). It appears to work satisfactorily and avoids the 55˚C water bath and extended incubation times required by other protocols. The authors say that no signal is lost following stripping, but that drying the blot at any stage does attenuate the signal; therefore, blots should be stored in TBS with 0.02% sodium azide in a sealed container.

- Following stripping, re-blocking is not necessary.
- The authors state that it is not suitable for nitrocellulose (50% of signal is lost).

Recipe

Stripping buffer	For 100ml
6M Guanidine Hydrochloride	57g Guanidine Hydrochloride
0.2% NP40	200µl NP40
20mM Tris-HCl pH 7.5	2ml 1M Tris-HCl pH7.5
	ddH_2O to 100ml; stir on stir plate until dissolved.
0.1M Beta mercaptoethanol	700µl 14.3M stock BME ***Add directly before use - see protocol; use 70µl per 10ml final.***

Store at room temperature without beta mercaptoethanol.

Protocol

1. Blot should be stored in buffer; if dry, re-wet in methanol, then TBS (or TBS-T). Rinse x2 in TBS-T if coming directly from ECL step of previous antibody.
2. Incubate blot in 10ml stripping buffer (with 70μl BME added per 10ml) for 5 minutes, shaking at room temperature. PVDF will become transparent (!).
3. Discard buffer and repeat step 2.
4. Rinse 4x in TBS-T, 3 minutes each to ensure all stripping buffer has been removed.
5. Proceed to primary antibody incubation step. Re-blocking is not necessary.

Assaying Topo IIα fragment DNA binding by oligo-coated bead pulldown

This protocol uses magnetic beads coated with oligonucleotides to assay DNA binding of proteins, in this case fragments of human Topoisomerase IIα or IIβ. By incubating DNA-coated beads with the protein of interest, washing the beads, and analyzing the bound fraction by Western blot, DNA/protein binding can be assessed. It is based on the protocol of (Wu, 2006), which was originally designed for assaying nuclear extract transcription factor binding to specific oligo sequences. This assay adapts the same protocol, but with modifications specific for use with purified protein preps rather than complex lysates. Specifically, use for this purpose required specific bead blocking steps to reduce/nearly eliminate nonspecific binding of protein to beads, at least for Topoisomerase IIα/β.

Blocking with 2% BSA was tried, but it was less effective in reducing background binding in the absence of DNA. Similarly, other detergents were tried, or at lower concentrations, but 1% NP40 was found to be optimal compared to lower concentrations.

Reagents required

Purified Topoisomerase II protein fragments
Streptavidin MagBeads (Cat #L00424, GenScript, Piscataway, NJ)
5' Biotin-labeled oligonucleotides (sense and antisense - see instructions below)

PBS
PBS-M10 buffer (see recipes)
PBS-M3 buffer
PBS-NP40 buffer

Magnetic separation rack (GenScript, Piscataway, NJ, or the more common Dynabeads rack from Invitrogen, Carlsbad, CA).
Rotating rack for incubation of 1.5ml tubes
Reagents and equipment for SDS-PAGE gels and Western blotting
Antibodies against protein of interest (e.g. Anti-HIS tag - see notes below)

Buffer compositions

PBS-M10: PBS + 10% instant dried milk + 1% NP40

PBS-M3: PBS + 3% instant dried milk + 1% NP40

PBS-NP40: PBS + 1% NP40

Oligo design, ordering and molarity calculations

For Topo IIα binding assays, oligos were ordered containing a 60bp fragment of pUC19 with the following sequence:

5' GGC CGA GCG CAG AAG TGG TCC TGC AAC TTT ATC CGC CTC CAT CCA GTC TAT TAA TTG TTG 3'

The reverse-compliment oligo was also ordered, and both forward and reverse were ordered as 5' biotinylated oligos on a 250nmole scale with standard desalting purification. The vendor used was the University of Minnesota Biomedical Genomics Center. The approximate cost was $90 for each oligo ($180 total). Note: similar results were obtained when only one oligo was biotinylated; the expense of biotinylating both sense and antisense may be unnecessary.

Oligos are individually resuspended in ddH_2O at a concentration of 1nmole/ul (i.e. 1mM ssDNA, also 1mM with respect to biotin)

For each sample, 20μl magnetic beads are used. For each protein to be tested, a sample of beads not bound to DNA (background control) is required in addition to a sample of beads streptavidin/biotin conjugated to oligos. Quantities are for each protein sample to be tested.

1. Wash 40μl bead suspension with PBS; split into two 1.5ml tubes in 500μl PBS. Label one "+ DNA" and one "- DNA".
2. Mix 10μl antisense biotinylated oligos with 10μl sense biotinylated oligos. To anneal, heat to 100˚C on heat block for 5 minutes and cool to room temperature.
3. Add oligos to "+ DNA". Rotate at room temperature, 30 minutes.
4. Using magnet, remove liquid from tubes containing beads.
5. Add 1ml PBS-M10 to each tube. Rotate at RT, 1hr.
6. Remove liquid using magnet again. Wash beads in PBS once. Resuspend in 500μl PBS-M3. Add 1.5μg protein of interest to each tube. Rotate at room temperature, up to 3 hours.
7. Wash beads x3 in PBS-NP40.
8. Analyze by western blot to protein of interest (anti-HIS antibody works well for pET-28a-expressed Topo IIα fragments.)

Lentiviral production

This procedure has several steps:

1. Ordering Lentiviral clones from BMGC
2. Making stocks of the clones
3. Preparing plasmid DNA from the clones
4. Preparing packaging plasmid DNA
5. Thawing and maintaining HEK 293T cells
6. Transfecting HEK 293T cells with packaging and shRNA plasmids and harvesting viral particles
7. Using prepared viral particles for knockdown in target cells

Ordering Lentiviral clones from BMGC

Note: the available clones are best browsed using the Open Biosystems website (openbiosystems.com). Search for your gene of interest in the gene search box, then, in the results page, click the **shRNA sets** tab. Then click **Change Filters**, then **Lentiviral,** then **pGIPZ**, then **Apply Filters**. You'll get two entries, usually, one for mouse and one for human-targed shRNAs. The GIPZ clone set all expresses a GFP marker for transduced cells, and they're the only ones we've used. They supposedly have the most "modern" (effective and specific, I guess) design for shRNAs, too. You can get vector maps and full instructions pretty easily by Googling for GIPZ, or browsing the Open Biosystems site.

1. Go to https://bmgcrnai.msi.umn.edu/cgi-bin/rnaidb.cgi
2. Search for your gene symbol. If it doesn't find it, you may have to get the NCBI accession number from the Open Biosystems site (e.g. NM_031965 for Haspin) and search on that instead.
3. Pick the ones you want, then add to cart - purchasing is pretty straightforward.
4. They're usually available for pickup the next day from the BMGC on the second floor of NHH. They come as agar stabs, and are apparently stable at 4˚C for months.

Making stocks of the clones

For this, you'll need:

LB + Amp plates.

Low-salt LB (LB with half the usual NaCl)

4000X Zeocin stock (100mg/ml)

1000X Ampicillin stock (100mg/ml)

1. Once you've got your clones, put a sterile pipette tip down into the agar stab, and streak onto an LB + Amp plate. Incubate at 37˚C overnight.
2. Pick a patch of your plate into about 2ml Low-Salt LB with Zeocin (25μg/ml) and Ampicillin (100μg/ml). Low-Salt LB is used because Zeocin is not active at high concentrations of NaCl.
3. Grow at 37˚C overnight.
4. Stock by adding glycerol to 20% final concentration and storing at -80˚C.

Preparing plasmid DNA from the clones

DNA is produced using standard methods. Cultures can be grown at 37˚C in regular LB containing Ampicillin at 100μg/ml; Zeocin is not necessary. Using ampicillin that has been repeatedly frozen and thawed has, in the past, resulted in problems preparing DNA from the cultures; there appears to be strong selection to lose the GIPZ plasmid, presumably because of its size. Furthermore, overnight cultures do not grow to an extremely high density, thus 10ml overnight culture per miniprep is preferable. Each miniprep tends to produce around 10-15ug plasmid.

Preparing packaging plasmid DNA

Two packaging plasmids are necessary for production of viral VSV-g pseudotyped lentiviral particles: pMDG (pAL340) and ΔNRF (pAL342), both AmpR. Prepare these either by pooling several minipreps or by using the Zymo Maxiprep kit (the Zymo Maxiprep kit is somewhat less expensive, per μg DNA, and appears to be more reliable than other large-scale kits).

Thawing and maintaining HEK 293T cells

HEK 293T cells are maintained in DMEM media + 10% FCS + 1% penicillin/ streptomycin solution. They grow quickly and probably only need to be thawed 3-4 days before viral production is started, depending on the amount of cells required. They do not adhere strongly to dishes and can be dissociated without trypsin (easily washed off with

DMEM from a 1ml pipette). Also, 10% FCS is probably unnecessary - 5% is probably fine.

Transfecting HEK 293T cells with packaging and shRNA plasmids and harvesting viral particles

Large amounts of viral particles can be produced easily. As a guideline, consider that each plate will produce [plate capacity in ml x 2] in viral supernatant. For example, a 10cm plate with 6ml media will produce 12ml total viral supernatant.

For most (e.g. timelapse) experiments, ~500ul is required per experiment, depending on the final titer. For protein extraction and chromosome spread experiments, much larger amounts of virus are necessary.

Day 1 Transfect plates that are approx. 70% confluent. For each shRNA to be produced, prepare tubes as follows. Tube B is the same for each shRNA, so can be made in one large batch.

Tube A	10cm plate	15cm plate
pGIPZ (shRNA plasmid)	8μg	20μg
ΔNRF	5.4μg	13.4μg
pMDG	2.7μg	6.7μg
Serum-free DMEM	600μl	1.5ml

Tube B (make as master mix)	10cm plate	15cm plate
PEI (Polyethylenimine, 1mg/ml in H2O)	50µl	120µl
Serum-free DMEM	600µl	1.5ml

Add tube B to tube A; vortex well. Incubate in hood for 20 minutes. Mix tube by pipetting up and down a few times, then add the mixture to plate of cells, drop by drop over plate surface. Place cells back in incubator overnight.

Day 2 **From here on, cells and media should be considered to contain active virus. Wear gloves**. Aspirate media into flask containing bleach. Replace with fresh DMEM/10% FCS/Antibiotics. To keep the virus particles as concentrated as possible, use the minimum amount of DMEM necessary to cover the cells (e.g. around 6ml for 10cm plate, 13ml for 15cm). The cells will be expressing GFP by now; this can be checked by putting the plate on the inverted scope under low power. If the cells are green at this point, but the final virus particles do not transduce, this suggests that either the pMDG or ΔNRF plasmid prep was bad.

Day 3 Harvest media containing virus particles into 15ml or 50ml tubes. Spin at 1500RPM, 2 minutes in bucket centrifuge to remove cells and debris; transfer supe to new 50ml tube and store at 4˚C overnight. Ideally, tubes should be in secondary containment to avoid contaminating refrigerator.

Day 4 Harvest media again. Spin again, combine with previous day's supernatant. Aliquot into sterile 1.5ml tubes (1ml each, or 400ul into 0.6ml tubes) and store directly at -80˚C.

Notes:

- Everything that comes into contact with virus particles should be either autoclaved or bleached for ~1h. If virus-containing media comes into contact with pipette handles, etc., spray down thoroughly with ethanol and allow to air dry.
- Virus particles can be concentrated in the ultracentrifuge at 20,000RPM for 1hr at 4˚C. However, this is inconvenient and usually unnecessary.
- Particles are apparently stable at 4˚C for a few days. If you're using them immediately, it may be better to avoid freezing them.
- Freeze/thaw cycles don't totally destroy the virus, but will thwart attempts to get reproducible results.

Using prepared viral particles for knockdown in target cells

For some uses, it may be sufficient to simply add a few hundred μl of thawed viral supernatant to cells growing in a tissue culture dish and incubate overnight. In this case, viral expression can be seen within 48h. However, for optimal transduction of cells, the following points are important:

- Cells can be trypsinized and re-seeded at desired density **at the same time** as adding virus. It is not necessary to wait for cells to attach to the dish.
- Add Polybrene (hexadimethrine bromide) to media at the time of transduction. 8μg/ml final; stock is 8mg/ml.
- Keeping constant the number of cells, the size of the dish and the volume of media all help to make the transduction reproducible.
- Titering virus can be carried out using an MTS assay and constructing a kill curve when cells are treated with puromycin at various concentrations of virus, assuming the virus has a drug resistance gene. From this kill curve, an approximate virus titer can be calculated.

Constructing FLP-in cell lines

A specific gene of interest can be inserted at a known locus using the HeLa EM2-11ht cell line characterized in (Weidenfeld et al., 2009). As of 3/2012, these cells are located in LN2-3C. These cells have the following characteristics and drug resistances:

EM2-11ht Cell line characteristics		
Feature	**Description**	**Resistance**
Advanced rtTA	Reverse Tet-transactivator (Tet-On) protein. Required for response to doxycycline.	G418 (400μg/ml)
FRT/F3 flp directional FLP recombinase sites	A pair of asymmetric recombination sites at a defined locus (see Weidenfeld et al., 2009), which can be induced to recombine with matching sites on a transfected plasmid when the FLP recombinase is co-transfected on an expression plasmid. See protocol.	N/A
hyg/TK cassette	This cassette containing two genes is situated between the FRT/F3 sites in the genome. It contains a positive and a negative selection marker, and is removed on successful insertion of your gene of interest.	hyg: Resistance to hygromycin (300μg/ml) TK: Confers **sensitivity** to ganciclovir (100μM). When removed, the cells are no longer sensitive to ganciclovir (although it still seems to be a bit toxic). The starting (EM2-11ht) cells are thus resistant to hygromycin and sensitive to ganciclovir.

Key S2F-IMCg plasmid characteristics	
Feature	**Description**
IMCg bidirectional promoter	Promoter that allows insertion of genes upstream and downstream of it under doxycycline inducible control.
F/F3 Recombination sites	Flank the insertion cassette; allow directional recombination of gene between them into HeLa-EM2-11ht genome

Protocol:

Day 0: Split HeLa-EM2-11ht into wells of a 6-well plate, $2.5x10^5$ cells/well, one well for each cell line to be constructed, plus two additional negative control wells. (Counting cells here may not be critical - suggest approx. 75% confluent).

Day 1: Change media on cells for fresh DMEM (+antibiotics, +FCS).

Prepare two tubes as follows :

Tube A (Transfection reagent)	Per well of 6-well plate
GenJet+	2µl
Serum-free DMEM	200µl

Tube A can be scaled up for the number of transfections to be carried out.

Tube B (DNA). Prepare for each clone to be transfected.		
Component	**Description**	**Per well of 6-well plate**
S2F vector	Gene of interest under Tet-regulatable promoter and flanked by recombination sites.	0.5μg
Flp-o (plasmid 422 in Andy's stocks)	FLP recombinase expression vector	1μg
pTRE-2 puro (plasmid 487 in Andy's stocks)	Puromycin resistance plasmid	0.5μg
Serum-free DMEM		200μl

In addition to the above, leave one negative control well untransfected. This will be used to test the efficiency of the initial Puromycin treatment. For the second control well, omit the Flp-O plasmid. This will provide a background number of colonies that arise in the absence of recombinase. Both controls are useful for troubleshooting.

Add Tube A to Tube B rapidly and mix immediately. Incubate at room temperature, 20 minutes. Add dropwise to cells, swirl, and place cells back in incubator.

Day 2: For each well of the 6-well dish, trypsinize and plate 50% of the cells into one 10cm dish, and 5% into a second 10cm dish. Add puromycin to each dish at a final concentration of 3.3μg/ml and incubate overnight.

Day 3: The puromycin treatment should have killed 100% of the control untransfected cells. Of the remaining dishes, most cells should be dead, but a large number of living

cells should remain adhered. Change the media again, this time without puromycin and with DMEM + FCS + antibiotics + 100μM ganciclovir (GCV).

Every two days from this point on: Change the media, using DMEM + FCS + antibiotics + 100μM ganciclovir. The ganciclovir may take 5-6 days to show an effect. As it begins to take effect, the cells will generate long projections. Eventually, the dish being to appear quite sick looking and it may appear as though all the cells are slowly dying and that no colonies are forming. However, around day 11-12, small colonies that are growing successfully should be apparent. Often they appear somewhat sick, even though they are growing. When picked/isolated and grown in the absence of ganciclovir, these colonies generally grow normally again.

Around Day 14: Colonies should be visible (size around 2-4mm) looking through the underside of the dish against the light. Pick clones using your preferred method. In general, around 50% of colonies are found to be expressing. Some of these clones appear not to grow robustly. It is suggested that around 24 colonies are picked to ensure at least 4-5 healthy, expressing clones are isolated. When expanded, split into two if desired and test one half for induction of the gene of interest on doxycycline addition.

Troubleshooting: If the protocol appears not to work, the mCherry or GFP expression S2F vectors can be used as a positive control. Doxycycline can be added to the plate containing colonies, and they can be examined through the plastic using the 20X objective on the Deltavision for expression.

mCherry-Topo IIα expression induced by Dox is barely visible in 50ng/ml Dox after 2-3 days. Expression maxes out (at still-not-very-bright) somewhere between 100ng/ml and 250ng/ml. In most rescue experiments, 250ng/ml was used.

References

Adolph, K.W. 1984. Conservation of interphase chromatin nonhistone antigens as components of metaphase chromosomes. *FEBS Lett*. 165:211–215.

Adolph, K.W., S.M. Cheng, J.R. Paulson, and U.K. Laemmli. 1977. Isolation of a protein scaffold from mitotic HeLa cell chromosomes. *Proc Natl Acad Sci USA*. 74:4937–4941.

Agostinho, M., J. Rino, J. Braga, F. Ferreira, S. Steffensen, and J. Ferreira. 2004. Human topoisomerase IIalpha: targeting to subchromosomal sites of activity during interphase and mitosis. *Mol Biol Cell*. 15:2388–2400.

Bekers, A.G., H.J. Gijzen, R.D. Taalman, and F. Wanka. 1981. Ultrastructure of the nuclear matrix from Physarum polycephalum during the mitotic cycle. *J. Ultrastruct. Res*. 75:352–362.

Belmont, A.S. 2002. Mitotic chromosome scaffold structure: new approaches to an old controversy. *Proc Natl Acad Sci USA*. 99:15855–15857.

Berezney, R., and D.S. Coffey. 1974. Identification of a nuclear protein matrix. *Biochem Bioph Res Co*. 60:1410–1417.

Capranico, G., S. Tinelli, C.A. Austin, M.L. Fisher, and F. Zunino. 1992. Different patterns of gene expression of topoisomerase II isoforms in differentiated tissues during murine development. *Biochimica et Biophysica Acta (BBA) - Gene Structure and Expression*. 1132:43–48.

Christensen, M.O., M.K. Larsen, H.U. Barthelmes, R. Hock, C.L. Andersen, E. Kjeldsen, B.R. Knudsen, O. Westergaard, F. Boege, and C. Mielke. 2002. Dynamics of human DNA topoisomerases IIalpha and IIbeta in living cells. *J Cell Biol*. 157:31–44.

Cokol, M., R. Nair, and B. Rost. 2000. Finding nuclear localization signals. *EMBO Rep*. 1:411–415.

Cuvier, O., and T. Hirano. 2003. A role of topoisomerase II in linking DNA replication to chromosome condensation. *J Cell Biol*. 160:645–655.

Dong, K.C., and J.M. Berger. 2007. Structural basis for gate-DNA recognition and bending by type IIA topoisomerases. *Nature*. 450:1201–1205.

Dorigo, B. 2004. Nucleosome Arrays Reveal the Two-Start Organization of the Chromatin Fiber. *Science*. 306:1571–1573.

Downes, C.S., D.J. Clarke, A.M. Mullinger, J.F. Giménez-Abián, A.M. Creighton, and R.T. Johnson. 1994. A topoisomerase II-dependent G2 cycle checkpoint in mammalian cells/. *Nature*. 372:467–470.

Earnshaw, W.C., B. Halligan, C.A. Cooke, M.M. Heck, and L.F. Liu. 1985. Topoisomerase II is a structural component of mitotic chromosome scaffolds. *J Cell Biol*. 100:1706–1715.

Engel, R., N.I. Valkov, J.L. Gump, L. Hazlehurst, W.S. Dalton, and D.M. Sullivan. 2004. The cytoplasmic trafficking of DNA topoisomerase IIalpha correlates with etoposide resistance in human myeloma cells. *Exp Cell Res*. 295:421–431.

Fachinetti, D., R. Bermejo, A. Cocito, S. Minardi, Y. Katou, Y. Kanoh, K. Shirahige, A. Azvolinsky, V.A. Zakian, and M. Foiani. 2010. Replication termination at eukaryotic chromosomes is mediated by Top2 and occurs at genomic loci containing pausing elements. *Mol Cell*. 39:595–605.

Finch, J.T., and A. Klug. 1976. Solenoidal model for superstructure in chromatin. *Proc Natl Acad Sci USA*. 73:1897–1901.

Giménez-Abián, J.F., and D.J. Clarke. 2009. Cytological analysis of chromosome structural defects that result from topoisomerase II dysfunction. *Methods Mol Biol*. 582:189–207.

Giménez-Abián, J.F., D.J. Clarke, A.M. Mullinger, C.S. Downes, and R.T. Johnson. 1995. A postprophase topoisomerase II-dependent chromatid core separation step in the formation of metaphase chromosomes. *J Cell Biol*. 131:7–17.

Grigoryev, S.A., G. Arya, S. Correll, C.L. Woodcock, and T. Schlick. 2009. Evidence for heteromorphic chromatin fibers from analysis of nucleosome interactions. *Proc Natl Acad Sci USA*. 106:13317–13322.

Hart, C.M., and U.K. Laemmli. 1998. Facilitation of chromatin dynamics by SARs. *Curr. Opin. Genet. Dev.* 8:519–525.

Hetzer, M., O.J. Gruss, and I.W. Mattaj. 2002. The Ran GTPase as a marker of chromosome position in spindle formation and nuclear envelope assembly. *Nat Cell Biol*. 4:E177.

Holm, C., T. Stearns, and D. Botstein. 1989. DNA topoisomerase II must act at mitosis to prevent nondisjunction and chromosome breakage. *Mol Cell Biol*. 9:159–168.

Jensen, S., A.H. Andersen, E. Kjeldsen, H. Biersack, E.H. Olsen, T.B. Andersen, O. Westergaard, and B.K. Jakobsen. 1996. Analysis of functional domain organization in DNA topoisomerase II from humans and Saccharomyces cerevisiae. *Mol Cell Biol*. 16:3866–3877.

Kaer, K., K. Mätlik, M. Metsis, and M. Speek. 2008. Combination of native and denaturing PAGE for the detection of protein binding regions in long fragments of genomic DNA. *BMC Genomics*. 9:272.

Kalab, P., A. Pralle, E.Y. Isacoff, R. Heald, and K. Weis. 2006. Analysis of a RanGTP-regulated gradient in mitotic somatic cells. *Nature*. 440:697–701.

LaCasse, E.C., and Y.A. Lefebvre. 1995. Nuclear localization signals overlap DNA- or RNA-binding domains in nucleic acid-binding proteins. *Nucleic Acids Res*. 23:1647–1656.

Langmore, J.P., and J.R. Paulson. 1983. Low angle x-ray diffraction studies of chromatin structure in vivo and in isolated nuclei and metaphase chromosomes. *J Cell Biol*. 96:1120–1131.

Linka, R.M., A.C.G. Porter, A. Volkov, C. Mielke, F. Boege, and M.O. Christensen. 2007. C-terminal regions of topoisomerase IIalpha and IIbeta determine isoform-specific functioning of the enzymes in vivo. *Nucleic Acids Res*. 35:3810–3822.

Losada, A., M. Hirano, and T. Hirano. 2002. Cohesin release is required for sister chromatid resolution, but not for condensin-mediated compaction, at the onset of mitosis. *Genes Dev*. 16:3004–3016.

Luger, K., A.W. Mäder, R.K. Richmond, D.F. Sargent, and T.J. Richmond. 1997. Crystal structure of the nucleosome core particle at 2.8 A resolution. *Nature*. 389:251–260.

Luo, K., J. Yuan, J. Chen, and Z. Lou. 2009. Topoisomerase IIalpha controls the decatenation checkpoint. *Nat Cell Biol*. 11:204–210.

Maeshima, K., and U.K. Laemmli. 2003. A two-step scaffolding model for mitotic chromosome assembly. *Dev Cell*. 4:467–480.

Maeshima, K., S. Hihara, and M. Eltsov. 2010. Chromatin structure: does the 30-nm fibre exist in vivo? *Curr Opin Cell Biol*. 22:291–297.

Mirski, S.E., J.H. Gerlach, and S.P. Cole. 1999. Sequence determinants of nuclear localization in the alpha and beta isoforms of human topoisomerase II. *Exp Cell Res*. 251:329–339.

Mirski, S.E.L., K.E. Sparks, B. Friedrich, M. Köhler, Y.-Y. Mo, W.T. Beck, and S.P.C. Cole. 2007. Topoisomerase II binds importin alpha isoforms and exportin/CRM1 but does not shuttle between the nucleus and cytoplasm in proliferating cells. *Exp Cell Res*. 313:627–637.

Mo, Y.Y., and W.T. Beck. 1999. Association of human DNA topoisomerase IIalpha with mitotic chromosomes in mammalian cells is independent of its catalytic activity. *Exp Cell Res*. 252:50–62.

Mullinger, A.M., and R.T. Johnson. 1979. The organization of supercoiled DNA from human chromosomes. *J Cell Sci*. 38:369–389.

Niimura, Y., and T. Gojobori. 2002. In silico chromosome staining: reconstruction of Giemsa bands from the whole human genome sequence. *Proc Natl Acad Sci USA*. 99:797–802.

Nishino, Y., M. Eltsov, Y. Joti, K. Ito, H. Takata, Y. Takahashi, S. Hihara, A.S. Frangakis, N. Imamoto, T. Ishikawa, and K. Maeshima. 2012. Human mitotic chromosomes consist predominantly of irregularly folded nucleosome fibres without a 30-nm chromatin structure. *EMBO J*.

Nitiss, J.L. 2009. DNA topoisomerase II and its growing repertoire of biological functions. *Nature Reviews Cancer*. 9:327–337.

Orrego, M., I. Ponte, A. Roque, N. Buschati, X. Mora, and P. Suau. 2007. Differential affinity of mammalian histone H1 somatic subtypes for DNA and chromatin. *BMC Biol*. 5:22.

Park, S.-W., A. Parrott, D. Fritz, Y. Park, M. Mathews, and C.-G. Lee. 2008. Regulation of the catalytic function of topoisomerase II alpha through association with RNA. *Nucleic Acids Res*. gkn614v1.

Paulson, J.R., and U.K. Laemmli. 1977. The structure of histone-depleted metaphase chromosomes. *Cell*. 12:817–828.

Robinson, P.J., and D. Rhodes. 2006. Structure of the “30nm” chromatin fibre: A key role for the linker histone. *Current Opinion in Structural Biology*. 16:336–343.

Saitoh, Y., and U.K. Laemmli. 1994. Metaphase chromosome structure: bands arise from a differential folding path of the highly AT-rich scaffold. *Cell*. 76:609–622.

Schalch, T., S. Duda, D.F. Sargent, and T.J. Richmond. 2005. X-ray structure of a tetranucleosome and its implications for the chromatin fibre. *Nat Cell Biol*. 436:138–141.

Strukov, Y.G., Y. Wang, and A.S. Belmont. 2003. Engineered chromosome regions with altered sequence composition demonstrate hierarchical large-scale folding within metaphase chromosomes. *J Cell Biol*. 162:23–35.

Szewczyk, B., and L.M. Kozloff. 1985. A method for the efficient blotting of strongly basic proteins from sodium dodecyl sulfate-polyacrylamide gels to nitrocellulose. *Anal Biochem*. 150:403–407.

Tahara, K., M. Takagi, M. Ohsugi, T. Sone, F. Nishiumi, K. Maeshima, Y. Horiuchi, N. Tokai-Nishizumi, F. Imamoto, T. Yamamoto, S. Kose, and N. Imamoto. 2008. Importin-beta and the small guanosine triphosphatase Ran mediate chromosome loading of the human chromokinesin Kid. *J Cell Biol*. 180:493–506.

Tavormina, P.A., M.-G. Côme, J.R. Hudson, Y.-Y. Mo, W.T. Beck, and G.J. Gorbsky. 2002. Rapid exchange of mammalian topoisomerase II alpha at kinetochores and chromosome arms in mitosis. *J Cell Biol*. 158:23–29.

Tennyson, R.B., and J.E. Lindsley. 1997. Type II DNA topoisomerase from Saccharomyces cerevisiae is a stable dimer. *Biochemistry*. 36:6107–6114.

Tseng, H., J.A. Biegel, and R.S. Brown. 1999. Basonuclin is associated with the ribosomal RNA genes on human keratinocyte mitotic chromosomes. *J Cell Sci*. 112 Pt 18:3039–3047.

Wang, J.C., 2002. Cellular roles of DNA topoisomerases: a molecular perspective. *Nat Rev Mol Cell Bio*. 3:430–440.

Weidenfeld, I., M. Gossen, R. Löw, D. Kentner, S. Berger, D. Görlich, D. Bartsch, H. Bujard, and K. Schönig. 2009. Inducible expression of coding and inhibitory RNAs from retargetable genomic loci. *Nucleic Acids Res*. 37:e50.

Wu, K.K. 2006. Analysis of protein-DNA binding by streptavidin-agarose pulldown. *Methods Mol Biol*. 338:281–290.

Yeung, Y.-G., and E.R. Stanley. 2009. A solution for stripping antibodies from polyvinylidene fluoride immunoblots for multiple reprobing. *Anal Biochem*. 389:89–91.

Appendix 1

Supplementary Figures

Histone modifications used on MODified histone peptide arrays		
Histones		
Histone H1		
Histone H2A		
Histone H2B		
Histone H3		
Histone H4		
Modifiable histone tail residues		
Name	**Abbreviation**	
Lysine	K	
Arginine	R	
Serine	S	
Threonine	T	
Modification		
Name	**Abbreviation**	**Applicable to**
Acetylation	ac	K
Monomethylation	me1	K
Dimethylation	me2	K
Trimethylation	me3	K
Symmetric dimethylation	me2s	R
Asymmetric dimethylation	me2a	R
Arginine citrullation	Cit	R
Phosphorylation	p	S,T
Example		
Histone H3, trimethylation on lysine 27	H3K27me3	

Table S1: Nomenclature used to abbreviate histone tail peptide modifications in MODified Histone peptide arrays.

Modified Histone H3 residues 1-19

A 1	A R T K Q T A R K S T G G K A P R K Q
A 2	A Rme2s T K Q T A R K S T G G K A P R K Q
A 3	A Rme2a T K Q T A R K S T G G K A P R K Q
A 4	A Cit T K Q T A R K S T G G K A P R K Q
A 5	A R pT K Q T A R K S T G G K A P R K Q
A 6	A R T Kme1 Q T A R K S T G G K A P R K Q
A 7	A R T Kme2 Q T A R K S T G G K A P R K Q
A 8	A R T Kme3 Q T A R K S T G G K A P R K Q
A 9	A R T Kac Q T A R K S T G G K A P R K Q
A10	A R T K Q T A Rme2s K S T G G K A P R K Q
A11	A R T K Q T A Rme2a K S T G G K A P R K Q
A12	A R T K Q T A Cit K S T G G K A P R K Q
A13	A R T K Q T A R Kme1 S T G G K A P R K Q
A14	A R T K Q T A R Kme2 S T G G K A P R K Q
A15	A R T K Q T A R Kme3 S T G G K A P R K Q
A16	A R T K Q T A R Kac S T G G K A P R K Q
A17	A R T K Q T A R K pS T G G K A P R K Q
A18	A R T K Q T A R K S pT G G K A P R K Q
A19	A R T K Q T A R K S T G G Kac A P R K Q
A20	A Rme2s pT K Q T A R K S T G G K A P R K Q
A21	A Rme2s T Kme1 Q T A R K S T G G K A P R K Q
A22	A Rme2s T Kme2 Q T A R K S T G G K A P R K Q
A23	A Rme2s T Kme3 Q T A R K S T G G K A P R K Q
A24	A Rme2s T Kac Q T A R K S T G G K A P R K Q
B 1	A Rme2a pT K Q T A R K S T G G K A P R K Q
B 2	A Rme2a T Kme1 Q T A R K S T G G K A P R K Q
B 3	A Rme2a T Kme2 Q T A R K S T G G K A P R K Q
B 4	A Rme2a T Kme3 Q T A R K S T G G K A P R K Q
B 5	A Rme2a T Kac Q T A R K S T G G K A P R K Q
B 6	A Cit pT K Q T A R K S T G G K A P R K Q
B 7	A Cit T Kme1 Q T A R K S T G G K A P R K Q
B 8	A Cit T Kme2 Q T A R K S T G G K A P R K Q
B 9	A Cit T Kme3 Q T A R K S T G G K A P R K Q
B10	A Cit T Kac Q T A R K S T G G K A P R K Q
B11	A R pT Kme1 Q T A R K S T G G K A P R K Q
B12	A R pT Kme2 Q T A R K S T G G K A P R K Q
B13	A R pT Kme3 Q T A R K S T G G K A P R K Q
B14	A R pT Kac Q T A R K S T G G K A P R K Q
B15	A Rme2s pT Kme1 Q T A R K S T G G K A P R K Q
B16	A Rme2s pT Kme2 Q T A R K S T G G K A P R K Q
B17	A Rme2s pT Kme3 Q T A R K S T G G K A P R K Q
B18	A Rme2s pT Kac Q T A R K S T G G K A P R K Q
B19	A Rme2a pT Kme1 Q T A R K S T G G K A P R K Q
B20	A Rme2a pT Kme2 Q T A R K S T G G K A P R K Q
B21	A Rme2a pT Kme3 Q T A R K S T G G K A P R K Q
B22	A Rme2a pT Kac Q T A R K S T G G K A P R K Q
B23	A R T K Q T A Rme2a Kme1 S T G G K A P R K Q
B24	A R T K Q T A Rme2a Kme2 S T G G K A P R K Q

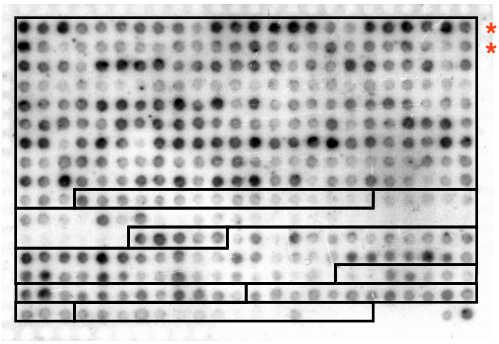

Figure S1: Annotated rows A and B of MODified Histone Array representing Histone H3 residues 1-19.

Modified Histone H3 residues 1-19

C 1	A R T K Q T A Rme2a Kme3 S T G G K A P R K Q
C 2	A R T K Q T A Rme2a Kac S T G G K A P R K Q
C 3	A R T K Q T A Rme2a K pS T G G K A P R K Q
C 4	A R T K Q T A Rme2a K S pT G G K A P R K Q
C 5	A R T K Q T A Rme2a Kme1 S T G G K A P R K Q
C 6	A R T K Q T A Rme2a Kme2 S T G G K A P R K Q
C 7	A R T K Q T A Rme2a Kme3 S T G G K A P R K Q
C 8	A R T K Q T A Rme2a Kac S T G G K A P R K Q
C 9	A R T K Q T A Rme2a K pS T G G K A P R K Q
C10	A R T K Q T A Rme2a K S pT G G K A P R K Q
C11	A R T K Q T A Cit Kme1 S T G G K A P R K Q
C12	A R T K Q T A Cit Kme2 S T G G K A P R K Q
C13	A R T K Q T A Cit Kme3 S T G G K A P R K Q
C14	A R T K Q T A Cit Kac S T G G K A P R K Q
C15	A R T K Q T A Cit K pS T G G K A P R K Q
C16	A R T K Q T A Cit K S pT G G K A P R K Q
C17	A R T K Q T A R Kme1 pS T G G K A P R K Q
C18	A R T K Q T A R Kme1 S pT G G K A P R K Q
C19	A R T K Q T A R Kme1 S T G G Kac A P R K Q
C20	A R T K Q T A R Kme2 pS T G G K A P R K Q
C21	A R T K Q T A R Kme2 S pT G G K A P R K Q
C22	A R T K Q T A R Kme2 S T G G Kac A P R K Q
C23	A R T K Q T A R Kme3 pS T G G K A P R K Q
C24	A R T K Q T A R Kme3 S pT G G K A P R K Q
D 1	A R T K Q T A R Kme3 S T G G Kac A P R K Q
D 2	A R T K Q T A R Kac pS T G G K A P R K Q
D 3	A R T K Q T A R Kac S pT G G K A P R K Q
D 4	A R T K Q T A R Kac S T G G Kac A P R K Q
D 5	A R T K Q T A R K pS pT G G K A P R K Q
D 6	A R T K Q T A R K pS T G G Kac A P R K Q
D 7	A R T K Q T A R K S pT G G Kac A P R K Q
D 8	A R T K Q T A Rme2s Kme1 pS T G G K A P R K Q
D 9	A R T K Q T A Rme2s Kme2 pS T G G K A P R K Q
D10	A R T K Q T A Rme2s Kme3 pS T G G K A P R K Q
D11	A R T K Q T A Rme2s Kac pS T G G K A P R K Q
D12	A R T K Q T A Rme2s Kme1 S pT G G K A P R K Q
D13	A R T K Q T A Rme2s Kme2 S pT G G K A P R K Q
D14	A R T K Q T A Rme2s Kme3 S pT G G K A P R K Q
D15	A R T K Q T A Rme2s Kac S pT G G K A P R K Q
D16	A R T K Q T A Rme2a Kme1 pS T G G K A P R K Q
D17	A R T K Q T A Rme2a Kme2 pS T G G K A P R K Q
D18	A R T K Q T A Rme2a Kme3 pS T G G K A P R K Q
D19	A R T K Q T A Rme2a Kac pS T G G K A P R K Q
D20	A R T K Q T A Rme2a Kme1 S pT G G K A P R K Q
D21	A R T K Q T A Rme2a Kme2 S pT G G K A P R K Q
D22	A R T K Q T A Rme2a Kme3 S pT G G K A P R K Q
D23	A R T K Q T A Rme2a Kac S pT G G K A P R K Q
D24	A R T K Q T A Rme2a Kme1 pS pT G G K A P R K Q

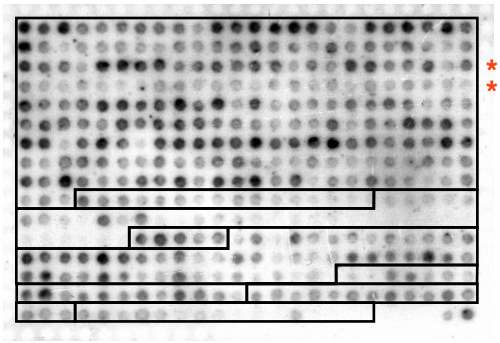

Figure S2: Annotated rows C and D of MODified Histone Array representing Histone H3 residues 1-19.

Modified Histone H3 residues 1-19

E 1	A R T K Q T A Rme2a Kme2 pS pT G G K A P R K Q
E 2	A R T K Q T A Rme2a Kme3 pS pT G G K A P R K Q
E 3	A R T K Q T A Rme2a Kac pS pT G G K A P R K Q
E 4	A Rme2s T Kme1 Q T A Rme2s K S T G G K A P R K Q
E 5	A Rme2s T Kme2 Q T A Rme2s K S T G G K A P R K Q
E 6	A Rme2s T Kme3 Q T A Rme2s K S T G G K A P R K Q
E 7	A Rme2s T Kac Q T A Rme2s K S T G G K A P R K Q
E 8	A Rme2a T Kme1 Q T A Rme2a K S T G G K A P R K Q
E 9	A Rme2a T Kme2 Q T A Rme2a K S T G G K A P R K Q
E10	A Rme2a T Kme3 Q T A Rme2a K S T G G K A P R K Q
E11	A Rme2a T Kac Q T A Rme2a K S T G G K A P R K Q
E12	A Rme2s T Kme1 Q T A R Kme1 S T G G K A P R K Q
E13	A Rme2s T Kme2 Q T A R Kme1 S T G G K A P R K Q
E14	A Rme2s T Kme3 Q T A R Kme1 S T G G K A P R K Q
E15	A Rme2s T Kac Q T A R Kme1 S T G G K A P R K Q
E16	A Rme2a T Kme1 Q T A R Kme2 S T G G K A P R K Q
E17	A Rme2a T Kme2 Q T A R Kme2 S T G G K A P R K Q
E18	A Rme2a T Kme3 Q T A R Kme2 S T G G K A P R K Q
E19	A Rme2a T Kac Q T A R Kme2 S T G G K A P R K Q
E20	A Rme2s T Kme1 Q T A R Kme3 S T G G K A P R K Q
E21	A Rme2s T Kme2 Q T A R Kme3 S T G G K A P R K Q
E22	A Rme2s T Kme3 Q T A R Kme3 S T G G K A P R K Q
E23	A Rme2s T Kac Q T A R Kme3 S T G G K A P R K Q
E24	A Rme2a T Kme1 Q T A R Kac S T G G K A P R K Q
F 1	A Rme2a T Kme2 Q T A R Kac S T G G K A P R K Q
F 2	A Rme2a T Kme3 Q T A R Kac S T G G K A P R K Q
F 3	A Rme2a T Kac Q T A R Kac S T G G K A P R K Q
F 4	A R T Kme1 Q T A Rme2s Kme1 S T G G K A P R K Q
F 5	A R T Kme2 Q T A Rme2s Kme1 S T G G K A P R K Q
F 6	A R T Kme3 Q T A Rme2s Kme1 S T G G K A P R K Q
F 7	A R T Kac Q T A Rme2s Kme1 S T G G K A P R K Q
F 8	A R T Kme1 Q T A Rme2a Kme1 S T G G K A P R K Q
F 9	A R T Kme2 Q T A Rme2a Kme1 S T G G K A P R K Q
F10	A R T Kme3 Q T A Rme2a Kme1 S T G G K A P R K Q
F11	A R T Kac Q T A Rme2a Kme1 S T G G K A P R K Q
F12	A R T Kme1 Q T A Rme2s Kme2 S T G G K A P R K Q
F13	A R T Kme2 Q T A Rme2s Kme2 S T G G K A P R K Q
F14	A R T Kme3 Q T A Rme2s Kme2 S T G G K A P R K Q
F15	A R T Kac Q T A Rme2s Kme2 S T G G K A P R K Q
F16	A R T Kme1 Q T A Rme2a Kme2 S T G G K A P R K Q
F17	A R T Kme2 Q T A Rme2a Kme2 S T G G K A P R K Q
F18	A R T Kme3 Q T A Rme2a Kme2 S T G G K A P R K Q
F19	A R T Kac Q T A Rme2a Kme2 S T G G K A P R K Q
F20	A R T Kme1 Q T A Rme2s Kme3 S T G G K A P R K Q
F21	A R T Kme2 Q T A Rme2s Kme3 S T G G K A P R K Q
F22	A R T Kme3 Q T A Rme2s Kme3 S T G G K A P R K Q
F23	A R T Kac Q T A Rme2s Kme3 S T G G K A P R K Q
F24	A R T Kme1 Q T A Rme2a Kme3 S T G G K A P R K Q

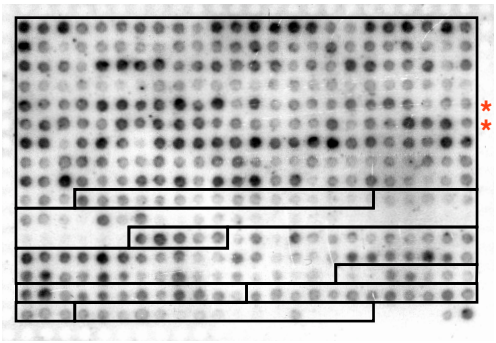

Figure S3: Annotated rows E and F of MODified Histone Array representing Histone H3 residues 1-19.

Modified Histone H3 residues 1-19

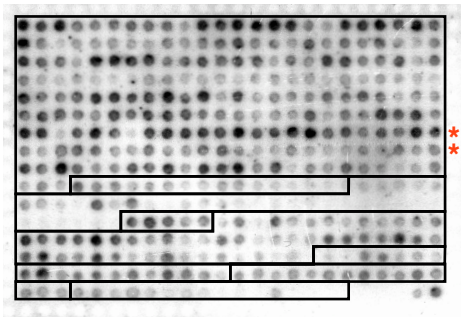

G 1	A R T Kme2 Q T A Rme2a Kme3 S T G G K A P R K Q
G 2	A R T Kme3 Q T A Rme2a Kme3 S T G G K A P R K Q
G 3	A R T Kac Q T A Rme2a Kme3 S T G G K A P R K Q
G 4	A R T Kme1 Q T A Rme2s Kac S T G G K A P R K Q
G 5	A R T Kme2 Q T A Rme2s Kac S T G G K A P R K Q
G 6	A R T Kme3 Q T A Rme2s Kac S T G G K A P R K Q
G 7	A R T Kac Q T A Rme2s Kac S T G G K A P R K Q
G 8	A R T Kme1 Q T A Rme2a Kac S T G G K A P R K Q
G 9	A R T Kme2 Q T A Rme2a Kac S T G G K A P R K Q
G10	A R T Kme3 Q T A Rme2a Kac S T G G K A P R K Q
G11	A R T Kac Q T A Rme2a Kac S T G G K A P R K Q
G12	A Rme2s T Kme1 Q T A Rme2s Kme1 S T G G K A P R K Q
G13	A Rme2s T Kme2 Q T A Rme2s Kme1 S T G G K A P R K Q
G14	A Rme2s T Kme3 Q T A Rme2s Kme1 S T G G K A P R K Q
G15	A Rme2s T Kac Q T A Rme2s Kme1 S T G G K A P R K Q
G16	A Rme2a T Kme1 Q T A Rme2s Kme1 S T G G K A P R K Q
G17	A Rme2a T Kme2 Q T A Rme2s Kme1 S T G G K A P R K Q
G18	A Rme2a T Kme3 Q T A Rme2s Kme1 S T G G K A P R K Q
G19	A Rme2a T Kac Q T A Rme2s Kme1 S T G G K A P R K Q
G20	A Rme2s T Kme1 Q T A Rme2s Kme2 S T G G K A P R K Q
G21	A Rme2s T Kme2 Q T A Rme2s Kme2 S T G G K A P R K Q
G22	A Rme2s T Kme3 Q T A Rme2s Kme2 S T G G K A P R K Q
G23	A Rme2s T Kac Q T A Rme2s Kme2 S T G G K A P R K Q
G24	A Rme2a T Kme1 Q T A Rme2s Kme2 S T G G K A P R K Q
H 1	A Rme2a T Kme2 Q T A Rme2s Kme2 S T G G K A P R K Q
H 2	A Rme2a T Kme3 Q T A Rme2s Kme2 S T G G K A P R K Q
H 3	A Rme2a T Kac Q T A Rme2s Kme2 S T G G K A P R K Q
H 4	A Rme2s T Kme1 Q T A Rme2s Kme3 S T G G K A P R K Q
H 5	A Rme2s T Kme2 Q T A Rme2s Kme3 S T G G K A P R K Q
H 6	A Rme2s T Kme3 Q T A Rme2s Kme3 S T G G K A P R K Q
H 7	A Rme2s T Kac Q T A Rme2s Kme3 S T G G K A P R K Q
H 8	A Rme2a T Kme1 Q T A Rme2s Kme3 S T G G K A P R K Q
H 9	A Rme2a T Kme2 Q T A Rme2s Kme3 S T G G K A P R K Q
H10	A Rme2a T Kme3 Q T A Rme2s Kme3 S T G G K A P R K Q
H11	A Rme2a T Kac Q T A Rme2s Kme3 S T G G K A P R K Q
H12	A Rme2s T Kme1 Q T A Rme2s Kac S T G G K A P R K Q
H13	A Rme2s T Kme2 Q T A Rme2s Kac S T G G K A P R K Q
H14	A Rme2s T Kme3 Q T A Rme2s Kac S T G G K A P R K Q
H15	A Rme2s T Kac Q T A Rme2s Kac S T G G K A P R K Q
H16	A Rme2a T Kme1 Q T A Rme2s Kac S T G G K A P R K Q
H17	A Rme2a T Kme2 Q T A Rme2s Kac S T G G K A P R K Q
H18	A Rme2a T Kme3 Q T A Rme2s Kac S T G G K A P R K Q
H19	A Rme2a T Kac Q T A Rme2s Kac S T G G K A P R K Q
H20	A Rme2s T Kme1 Q T A Rme2a Kme1 S T G G K A P R K Q
H21	A Rme2s T Kme2 Q T A Rme2a Kme1 S T G G K A P R K Q
H22	A Rme2s T Kme3 Q T A Rme2a Kme1 S T G G K A P R K Q
H23	A Rme2s T Kac Q T A Rme2a Kme1 S T G G K A P R K Q
H24	A Rme2a T Kme1 Q T A Rme2a Kme1 S T G G K A P R K Q

Figure S4: Annotated rows G and H of MODified Histone Array representing Histone H3 residues 1-19.

Modified Histone H3 residues 1-19

I 1	A Rme2a T Kme2 Q T A Rme2a Kme1 S T G G K A P R K Q
I 2	A Rme2a T Kme3 Q T A Rme2a Kme1 S T G G K A P R K Q
I 3	A Rme2a T Kac Q T A Rme2a Kme1 S T G G K A P R K Q
I 4	A Rme2s T Kme1 Q T A Rme2a Kme2 S T G G K A P R K Q
I 5	A Rme2s T Kme2 Q T A Rme2a Kme2 S T G G K A P R K Q
I 6	A Rme2s T Kme3 Q T A Rme2a Kme2 S T G G K A P R K Q
I 7	A Rme2s T Kac Q T A Rme2a Kme2 S T G G K A P R K Q
I 8	A Rme2a T Kme1 Q T A Rme2a Kme2 S T G G K A P R K Q
I 9	A Rme2a T Kme2 Q T A Rme2a Kme2 S T G G K A P R K Q
I10	A Rme2a T Kme3 Q T A Rme2a Kme2 S T G G K A P R K Q
I11	A Rme2a T Kac Q T A Rme2a Kme2 S T G G K A P R K Q
I12	A Rme2s T Kme1 Q T A Rme2a Kme3 S T G G K A P R K Q
I13	A Rme2s T Kme2 Q T A Rme2a Kme3 S T G G K A P R K Q
I14	A Rme2s T Kme3 Q T A Rme2a Kme3 S T G G K A P R K Q
I15	A Rme2s T Kac Q T A Rme2a Kme3 S T G G K A P R K Q
I16	A Rme2a T Kme1 Q T A Rme2a Kme3 S T G G K A P R K Q
I17	A Rme2a T Kme2 Q T A Rme2a Kme3 S T G G K A P R K Q
I18	A Rme2a T Kme3 Q T A Rme2a Kme3 S T G G K A P R K Q
I19	A Rme2a T Kac Q T A Rme2a Kme3 S T G G K A P R K Q
I20	A Rme2s T Kme1 Q T A Rme2a Kac S T G G K A P R K Q
I21	A Rme2s T Kme2 Q T A Rme2a Kac S T G G K A P R K Q
I22	A Rme2s T Kme3 Q T A Rme2a Kac S T G G K A P R K Q
I23	A Rme2s T Kac Q T A Rme2a Kac S T G G K A P R K Q
I24	A Rme2a T Kme1 Q T A Rme2a Kac S T G G K A P R K Q
J 1	A Rme2a T Kme2 Q T A Rme2a Kac S T G G K A P R K Q
J 2	A Rme2a T Kme3 Q T A Rme2a Kac S T G G K A P R K Q
J 3	A Rme2a T Kac Q T A Rme2a Kac S T G G K A P R K Q

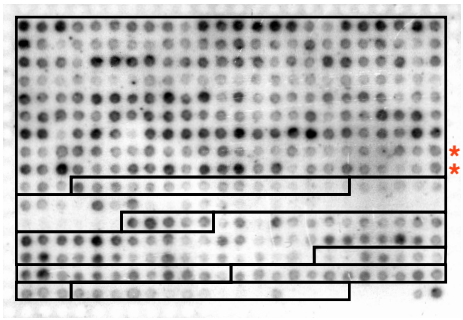

Figure S5: Annotated rows I and J of MODified Histone Array representing Histone H3 residues 1-19.

Modified Histone H3 residues 7-26

J 4	A R K S T G G K A P R K Q L A T K A A R
J 5	A R K S T G G Kac A P R K Q L A T K A A R
J 6	A R K pS T G G Kac A P R K Q L A T K A A R
J 7	A R K S pT G G Kac A P R K Q L A T K A A R
J 8	A R K S T G G K A P Rme2s K Q L A T K A A R
J 9	A R K S T G G K A P Rme2a K Q L A T K A A R
J10	A R K S T G G K A P Cit K Q L A T K A A R
J11	A R K S T G G K A P R Kac Q L A T K A A R
J12	A R K S T G G Kac A P Rme2s K Q L A T K A A R
J13	A R K S T G G Kac A P Rme2a K Q L A T K A A R
J14	A R K S T G G Kac A P R Kac Q L A T K A A R
J15	A R K S T G G K A P Rme2s Kac Q L A T K A A R
J16	A R K S T G G K A P Rme2a Kac Q L A T K A A R
J17	A R K S T G G K A P Cit Kac Q L A T K A A R
J18	A R K S T G G Kac A P Rme2s Kac Q L A T K A A R
J19	A R K S T G G Kac A P Rme2a Kac Q L A T K A A R

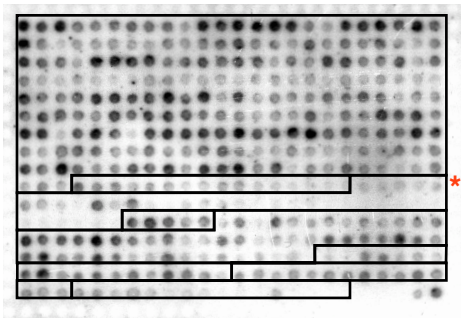

Figure S6: Annotated partial row J of MODified Histone Array representing Histone H3 residues 7-26

Modified Histone H3 residues 26-45

L 7 R K S A P A T G G V K K P H R Y R P G
L 8 R K S A P A T G G V Kme1 K P H R Y R P G
L 9 R K S A P A T G G V Kme2 K P H R Y R P G
L10 R K S A P A T G G V Kme3 K P H R Y R P G
L11 R K S A P A T G G V Kac K P H R Y R P G

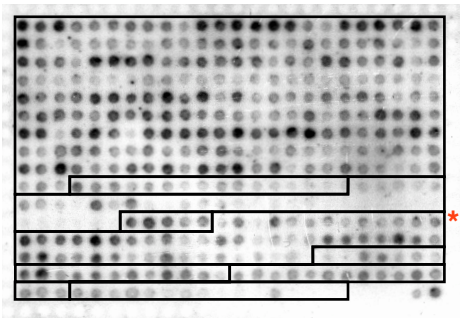

Figure S7: Annotated partial row L of MODified Histone Array representing Histone H3 residues 26-45

Modified Histone H4 residues 1-19

L12	S G R G K G G K G L G K G G A K R H R
L13	pS G R G K G G K G L G K G G A K R H R
L14	S G Rme2s G K G G K G L G K G G A K R H R
L15	S G Rme2a G K G G K G L G K G G A K R H R
L16	S G R G Kac G G K G L G K G G A K R H R
L17	S G R G K G G Kac G L G K G G A K R H R
L18	S G R G K G G K G L G Kac G G A K R H R
L19	S G R G K G G K G L G K G G A Kac R H R
L20	pS G Rme2s G K G G K G L G K G G A K R H R
L21	pS G Rme2a G K G G K G L G K G G A K R H R
L22	pS G R G Kac G G K G L G K G G A K R H R
L23	S G Rme2s G Kac G G K G L G K G G A K R H R
L24	S G Rme2s G K G G Kac G L G K G G A K R H R
M 1	S G Rme2a G Kac G G K G L G K G G A K R H R
M 2	S G Rme2a G K G G Kac G L G K G G A K R H R
M 3	S G R G Kac G G Kac G L G K G G A K R H R
M 4	S G R G K G G Kac G L G Kac G G A K R H R
M 5	S G R G K G G Kac G L G K G G A Kac R H R
M 6	S G R G K G G K G L G Kac G G A Kac R H R
M 7	pS G Rme2s G Kac G G K G L G K G G A K R H R
M 8	pS G Rme2a G Kac G G K G L G K G G A K R H R
M 9	S G Rme2s G Kac G G Kac G L G K G G A K R H R
M10	S G Rme2a G Kac G G Kac G L G K G G A K R H R
M11	S G R G Kac G G Kac G L G Kac G G A K R H R
M12	S G R G K G G Kac G L G Kac G G A Kac R H R
M13	pS G Rme2s G Kac G G Kac G L G K G G A K R H R
M14	pS G Rme2a G Kac G G Kac G L G K G G A K R H R
M15	S G Rme2s G Kac G G Kac G L G Kac G G A K R H R
M16	S G Rme2a G Kac G G Kac G L G Kac G G A K R H R
M17	S G R G Kac G G Kac G L G Kac G G A Kac R H R

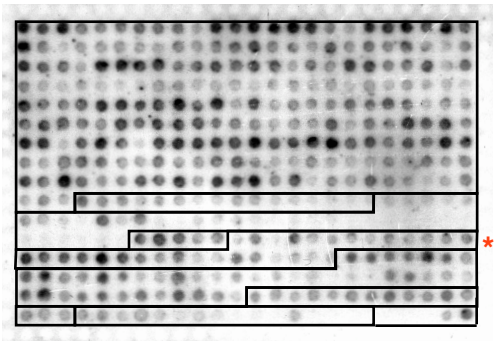

Figure S8: Annotated partial rows L and M of MODified Histone Array representing Histone H4 residues 1-19.

Modified Histone H4 residues 11-30

M18	G K G G A K R H R K V L R D N I Q G I T
M19	G Kac G G A K R H R K V L R D N I Q G I T
M20	G K G G A Kac R H R K V L R D N I Q G I T
M21	G K G G A K Rme2s H R K V L R D N I Q G I T
M22	G K G G A K Rme2a H R K V L R D N I Q G I T
M23	G K G G A K R H Rme2s K V L R D N I Q G I T
M24	G K G G A K R H Rme2a K V L R D N I Q G I T
N 1	G K G G A K R H R Kme1 V L R D N I Q G I T
N 2	G K G G A K R H R Kme2 V L R D N I Q G I T
N 3	G K G G A K R H R Kme3 V L R D N I Q G I T
N 4	G K G G A K R H R Kac V L R D N I Q G I T
N 5	G K G G A K R H R K V L Rme2a D N I Q G I T
N 6	G K G G A K R H R K V L Rme2s D N I Q G I T
N 7	G Kac G G A Kac R H R K V L R D N I Q G I T
N 8	G K G G A Kac Rme2s H R K V L R D N I Q G I T
N 9	G K G G A Kac Rme2a H R K V L R D N I Q G I T
N10	G K G G A Kac R H Rme2s K V L R D N I Q G I T
N11	G K G G A Kac R H Rme2a K V L R D N I Q G I T
N12	G K G G A Kac R H R Kme1 V L R D N I Q G I T
N13	G K G G A Kac R H R Kme2 V L R D N I Q G I T
N14	G K G G A Kac R H R Kme3 V L R D N I Q G I T
N15	G K G G A Kac R H R Kac V L R D N I Q G I T
N16	G Kac G G A Kac R H R Kme1 V L R D N I Q G I T
N17	G Kac G G A Kac R H R Kme2 V L R D N I Q G I T
N18	G Kac G G A Kac R H R Kme3 V L R D N I Q G I T
N19	G Kac G G A Kac R H R Kac V L R D N I Q G I T
N20	G K G G A K R H Rme2a Kme1 V L R D N I Q G I T
N21	G K G G A K R H Rme2a Kme2 V L R D N I Q G I T
N22	G K G G A K R H Rme2a Kme3 V L R D N I Q G I T
N23	G K G G A K R H Rme2a Kac V L R D N I Q G I T
N24	G K G G A K R H Rme2s Kme1 V L R D N I Q G I T
O 1	G K G G A K R H Rme2s Kme2 V L R D N I Q G I T
O 2	G K G G A K R H Rme2s Kme3 V L R D N I Q G I T
O 3	G K G G A K R H Rme2s Kac V L R D N I Q G I T
O 4	G K G G A K R H R Kme1 V L Rme2a D N I Q G I T
O 5	G K G G A K R H R Kme2 V L Rme2a D N I Q G I T
O 6	G K G G A K R H R Kme3 V L Rme2a D N I Q G I T
O 7	G K G G A K R H R Kac V L Rme2a D N I Q G I T
O 8	G K G G A K R H R Kme1 V L Rme2s D N I Q G I T
O 9	G K G G A K R H R Kme2 V L Rme2s D N I Q G I T
O10	G K G G A K R H R Kme3 V L Rme2s D N I Q G I T
O11	G K G G A K R H R Kac V L Rme2s D N I Q G I T

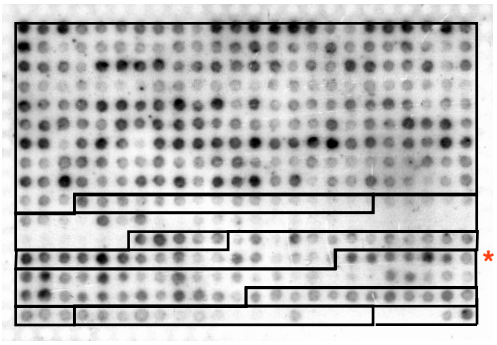

Figure S9: Annotated partial rows M, N and O of MODified Histone Array representing Histone H4 residues 11-30.

Modified Histone H2A residues 1-19

O12	S G R G K Q G G K A R A K A K S R S S
O13	pS G R G K Q G G K A R A K A K S R S S
O14	S G R G Kac Q G G K A R A K A K S R S S
O15	S G R G K Q G G Kac A R A K A K S R S S
O16	S G R G K Q G G K A R A Kac A K S R S S
O17	pS G R G Kac Q G G K A R A K A K S R S S
O18	pS G R G K Q G G Kac A R A K A K S R S S
O19	pS G R G K Q G G K A R A Kac A K S R S S
O20	S G R G Kac Q G G Kac A R A K A K S R S S
O21	S G R G Kac Q G G K A R A Kac A K S R S S
O22	S G R G K Q G G Kac A R A Kac A K S R S S
O23	pS G R G Kac Q G G Kac A R A K A K S R S S
O24	pS G R G Kac Q G G K A R A Kac A K S R S S
P 1	pS G R G K Q G G Kac A R A Kac A K S R S S
P 2	S G R G Kac Q G G Kac A R A Kac A K S R S S
P 3	pS G R G Kac Q G G Kac A R A Kac A K S R S S

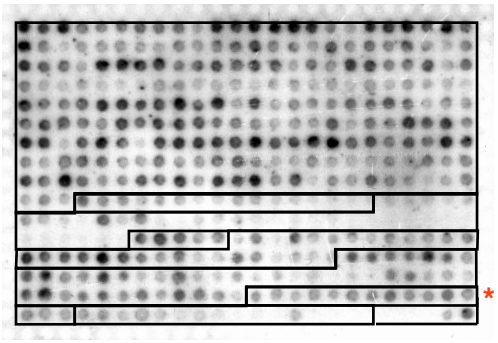

Figure S10: Annotated partial rows O and P of MODified Histone Array representing Histone H2A residues 1-19.

Modified Histone H2B residues 1-19

P 4	P D P A K S A P A P K K G S K K A V T
P 5	P D P A Kac S A P A P K K G S K K A V T
P 6	P D P A K S A P A P K Kac G S K K A V T
P 7	P D P A K S A P A P K K G pS K K A V T
P 8	P D P A K S A P A P K K G S Kac K A V T
P 9	P D P A Kac S A P A P K Kac G S K K A V T
P10	P D P A Kac S A P A P K K G pS K K A V T
P11	P D P A Kac S A P A P K K G S Kac K A V T
P12	P D P A K S A P A P K Kac G pS K K A V T
P13	P D P A K S A P A P K Kac G S Kac K A V T
P14	P D P A K S A P A P K K G pS Kac K A V T
P15	P D P A Kac S A P A P K Kac G pS K K A V T
P16	P D P A Kac S A P A P K Kac G S Kac K A V T
P17	P D P A Kac S A P A P K K G pS Kac K A V T
P18	P D P A K S A P A P K Kac G pS Kac K A V T
P19	P D P A Kac S A P A P K Kac G pS Kac K A V T

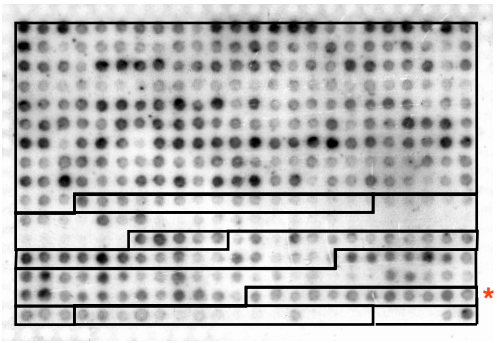

Figure S11: Annotated partial row P of MODified Histone Array representing Histone H2B residues 1-19

Appendix 2

Reagent locations in lab

Biotinylated oligos: In box in upright -20 with “Protein samples and Antibodies”. Tubes have blue caps.

Ganciclovir: Box on top shelf of -80, second rack from the left, near back. Blue plastic, says, Ganciclovir and PEI stocks.

PEI (Polyethylenimine): Box on top shelf of -80, second rack from the left, near back. Blue plastic, says, Ganciclovir and PEI stocks.

Polybrene: Tissue culture -20˚C. In gray plastic box, in small blue 0.6ml tubes at 8mg/ml. Throw away aliquots after thawing. New powder is in door of tissue culture 4˚C (make up in water to 8mg/ml, filter, then freeze).

Nocodazole: Chest -20. In a box that says “Laura’s Mammalian Antibodies”; orange-capped tubes.

Topo IIα-specific antibody. In box in deli fridge, Santa Cruz H-231.

α-Tubulin antibody. In -20, antibody #37. Or aliquot in box in deli fridge.